Efficient Electronic Communication of Two Ruthenium Centers through a Rigid Ditopic N-Heterocyclic Carbene Linker

Michael Nussbaum,[a] Oliver Schuster,*[a] Martin Albrecht*[a,b]

[a] *Department of Chemistry, University of Fribourg, Chemin du Musée 9, CH-1700 Fribourg, Switzerland*

[b] *School of Chemistry & Chemical Biology, University College Dublin, Belfield, Dublin 4, Ireland.*

Fax: +35317162501; Phone: +35317162504; E-mail: martin.albrecht@ucd.ie

Abstract. A ditopic benzobis(carbene) ligand precursor was prepared that contained a chelating pyridyl moiety to ensure co-planarity of the carbene ligand and the coordination plane of a bound octahedral metal center. Bimetallic ruthenium complexes comprising this ditopic ligand L_4Ru–*C,N*–bbi–*C,N*–RuL_4 were obtained by a transmetalation methodology (*C,N*–bbi–*C,N* = benzobis(*N*-pyridyl-*N*'-methyl-imidazolylidene). The two metal centers are electronically decoupled when the ruthenium is in a pseudo-tetrahedral geometry imparted by a cymene spectator ligand (L_4 = [(cym)Cl]). Ligand exchange of the Cl^-/cymene ligands for two bipyridine or four MeCN ligands induced a change of the coordination geometry to octahedral. As a consequence, the ruthenium centers, separated through space by more than 10 Å, become electronically coupled, which is evidenced by two distinctly different metal-centered oxidation processes that are separated by 134 mV (L_4 = [$(bpy)_2$]) and 244 mV (L_4 = [$(MeCN)_4$]), respectively. Hush analysis of the intervalence charge transfer bands in the mixed-valent species indicates substantial valence delocalization in both complexes (delocalization parameter Γ = 0.41 and 0.37 in the bpy and MeCN complexes, respectively). Spectroelectrochemical measurements further indicated that the mixed-valent Ru^{II}/Ru^{III} species and the fully oxidized Ru^{III}/Ru^{III} complexes gradually decompose when bound to MeCN ligands, while the bpy spectators significantly enhance the stability. These results demonstrate the efficiency of carbenes and in particular of the bbi ligand scaffold for mediating electron transfer and for the fabrication of molecular redox switches. Moreover, the relevance of spectator ligands is emphasized for tailoring the degree of electronic communication through the benzobis(carbene) linker.

Introduction

Molecular switches provide intriguing opportunities as active entities for the storage and processing of data.[1] Metal complexes are particularly attractive units for such switching purposes, since they offer multiple read-out functions due to their potential activity in non-invasive events such as reversible redox,[2] spin transitions,[3] and charge transfer[4] processes. The resulting electronic, magnetic and optical signals constitute a diagnostic probe for the state of the switch.[1–4] The information density can be considerably enhanced when metal centers are mutually coupled. For example, redox switching of a bimetallic species gives access to a stable mixed-valent state in addition to the fully oxidized and reduced states, if the metal centers are electronically coupled.[5] Such mixed-valent states have distinct properties that depend on the degree of coupling.[6] A valence-localized system will thus provide access to a molecular diode with the oxidized entity as acceptor and the reduced unit as donor site.[7] Valence-delocalized systems will be excellent constituents of molecular wires[8] with the possibility for tailoring activity through modification of the bridging ligand.

Intramolecular metal-metal coupling is critically dependent on the ability of the bridging ligand to function as an electronic relay.[9] The two currently most popular classes of ligands that promote coupling in bimetallic systems are comprised of either ditopic bi- and oligopyridines,[10] and of oliogacetylenes.[11] While the latter type of ligands offers an excellent electronic link between the metal and the bridging ligand with a high degree of d_M–π_L overlap, especially in metal-alkylidene and metal-alkynylidene oxidation states, the oligopyridine family dwells on the π-acidity of the chelating pyridyl ligand and its synthetic versatility for functionalization. In a simplistic view, N-heterocyclic carbenes (NHCs)[12] represent a fusion of these two successful classes of ligands, featuring the synthetic versatility[13] of pyridines with the (partial) π component of the M–C_{NHC} bond[14] reminiscent of acetylenes. Stimulated by these considerations, a variety of ditopic NHC ligands have been developed (*e.g.* **A–C**, Fig. 1).[15] However, even in complexes containing the apparently highly conjugated benzobis(imidazolylidene) bridging ligand **C**, the metal-metal interaction was mediocre at best. Different explanations for the weak coupling of the metal centers in this molecular configuration have been put forward,[16] including low d_M–π_L overlap due to a mismatch of the ligand 2p orbital and the metal 4d orbitals,[17] poor π electron delocalization between the arene and the NCN units in the bridging ligand,[18] and an unfavorable orientation of the relevant d_M orbitals with respect to the π_L system that mimizes overlap.[19] We have addressed this latter issue by incorporating rigid pyridyl donor groups into the NHC wingtips,

which induce chelation and consequentially impart a coaxial arrangement of the metal and ligand orbitals, a concept that has been widely exploited in bipyridine chemistry.[20] The constrained NHC coordination substantially enhances the intermetallic coupling between two ruthenium centers bridged by ligands of type **C**. The electronic Ru…Ru coupling is critically dependent on the nature of the spectator ligands and on the coordination geometry they impose. These results indicate that appropriately designed dicarbenes provide efficient bridging ligands for the fabrication of molecular switches, and they emphasize the relevance of the mutual orientation of ligand and metal orbitals.

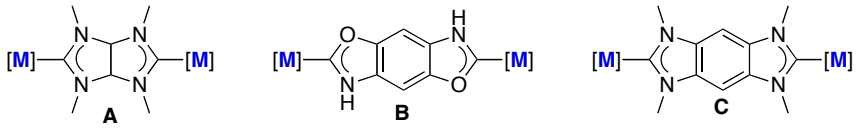

Fig 1. Relevant examples of ditopic NHC ligands.

Results and discussion

Synthesis of ditopic pyridyl-carbene precursor and dimetallic Ru_2 complexes. The synthetic approach towards chelating dicarbene ligands containing pyridyl donor groups was inspired by a methodology developed by Bielawski and coworkers for related monodentate ligand platforms (Scheme 1).[21] Accordingly, amination of 2,4-dinitro-1,5-dichlorobenzene with 2-aminopyridine furnished the pyridyl-functionalized product **1**. Aminations performed in EtOH at 120 °C afforded **1** only after extended reaction times and furnished monosubstituted compounds as major products due presumably to the deactivating effect of the first pyridyl substituent. Yields and purity were substantially higher in a solvent-free reaction using a large excess of 2-aminopyridine at 90 °C. Subsequent heterocycle formation was achieved in a palladium-catalyzed one-pot reaction involving reduction of the nitro groups with formic acid followed by *in situ* cyclization with orthoformate, which afforded the pyridyl-substituted benzobis(imidazole) **2**. Cyclization induced a marked upfield shift of the aryl proton resonances from δ_H 9.38 and 10.26 in **1** to 8.32 and 8.92 ppm in **2**. Moreover, a singlet at δ_H 8.62 ppm was attributed to the imidazole proton (δ_C 142.2 ppm). The reaction proceeds in high yields (>80%). The largest side product was identified by HPLC-MS (m/z 357 g mol^{-1}) as an ethoxy-adduct of **2**, possibly originating from incomplete EtOH elimination upon cyclization with $HC(OEt)_3$. Formation of **2** was unambiguously confirmed

by an X-ray crystal structure determination (Fig. S1), which revealed an essentially planar molecular structure for **2**. The central benzene ring is elongated along the CH…CH vector, a feature that was previously observed by Bielawski[xx] and us,[xx] albeit in a less pronounced manner. Pairs of molecules of **2** are stacked along the crystallographic c-axis and give rise to supramolecular zig-zag layers in the a-b plane (Fig. S1).

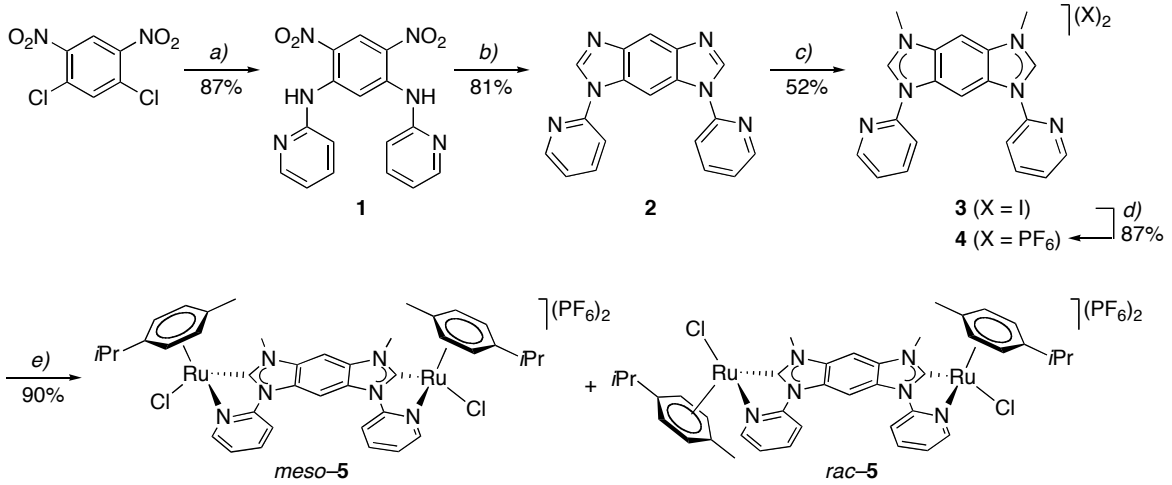

Scheme 1. Synthesis of complexes **5**. *Reagents and conditions*: a) 2-NH_2–pyridine, 90 °C, 3 d; b) HCOONa, HCOOH, Pd/C, $HC(OEt)_3$, 100 °C, 36 h; c) MeI, MeCN, microwave irradiation, 110 °C, 1 h; d) $(NH_4)PF_6$, H_2O; e) Ag_2O, MeOH, 24 h, then $[RuCl_2(p\text{-cymene})]_2$, CH_2Cl_2, 3 d; f) $AgPF_6$, MeCN, reflux, 20 h (52%); g) 2,2'-bipyridine, $MeNO_2$, reflux, 20 h.

The benzobis(imidazole) was selectively quaternized with excess MeI to yield the benzobis(imidazolium) salt **3**. The substantial downfield shift of the NCHN proton (from δ_H 8.62 to 10.84 ppm) and to a lesser extent of the aryl protons ($\Delta\delta$ ca. 0.8 ppm) in the ^1H NMR spectrum supports alkylation of the imidazole unit. Moreover, the NMR resonances of the pyridyl fragment are essentially unaltered upon alkylation, indicating that imidazole methylation is selective. Anion exchange with aqueous $(NH_4)PF_6$ gave **4** and was carried out to avoid issues due to potential halide scrambling in the subsequent (trans)metallation step.

Complexation of the ditopic carbene precursor was accomplished according to a classical metalation-transmetalation protocol using Ag_2O and $[RuCl_2(\eta^6\text{-p-cymene})]_2$.[22] While the transruthenation afforded pure products when performed in CH_2Cl_2, reaction with Ag_2O in this solvent was exceedingly slow, presumably due to the limited solubility of the dicationic salt **4**. Therefore, formation of the carbene silver intermediate was performed in MeOH and the solvent was then changed to CH_2Cl_2 for the transmetalation, without any purification or characterization of the probably polymeric silver complex.[23] Complex **5** is an air stable orange solid. While HPLC-MS suggests a pure compound, NMR analysis shows two distinct sets of signals that were attributed to the *rac* and *meso* diastereoisomers of **5** as a consequence

of the chirality of the complex at each ruthenium center.[15,24] Solubility tests revealed that one of the two isomers is less soluble in MeCN and was thus successfully separated by repetitive precipitation and filtration. This isomer is stable in solution over several days, demonstrating that racemization at ruthenium is very slow. Hence, 2D NMR measurements allowed all resonances to be assigned to one or the other isomer. However, we were unable to confidently assign the *meso* and *rac* designations based on spectroscopic data, and crystallization attempts have failed to date.

Successful double metalation was indicated by the pertinent cymene/benzobis(carbene) integral ratios and by the carbenic resonance at δ_C 202.8 and 203.3 ppm, corresponding to more than 50 ppm downfield shift compared to the ligand precursor (Table 1). As expected for a chiral complex, all four aromatic cymene protons are magnetically inequivalent, and the *i*Pr group appears as two distinct high field doublets for each isomer. Chelation of the pyridyl group is supported by the marked deshielding of the C6-bound pyridyl protons ($\Delta\delta$ > 0.4 ppm). Moreover, the resonances of the protons of the central arene ring experience a diagnostic upfield shift upon ruthenation and appear at δ_H 7.84 and 7.69 ppm in one isomer, and at δ_H 8.20 and 8.56 ppm in the other one (*cf* δ_H 9.08 and 9.65 ppm in the ligand precursor **4**). These shift differences suggest a strong electronic coupling of the metal center with the central arene moiety.

Table 1. Selected NMR shifts of complexes **5**–**7** and the ligand precursor **4** [a)]

Compound	δ_C NCN	δ_H H_{Ar}	δ_C C_{Ar}–H	δ_H $H_{Ar'}$	δ_C $C_{Ar'}$
4	146.7	9.65	103.6	9.08	99.7
5	203.3	8.56	97.8	8.20	96.7
5'	202.8	7.84	95.9	7.69	95.9
6	207.6	8.58	95.9	8.11	94.8
7	211.1	8.92	96.2	7.69	93.7

a) all data in $CDCl_3$ except **4** (in DMSO–d_6); Ar denotes the position β to the pyridyl-substituted nitrogen, Ar' the position β to the methyl-substituted nitrogen atom; **5** and **5'** are the two diastereoisomers of **5** (*meso* and *rac*).

Substitution of the ancillary ligands was achieved according to established procedures.[25] Thus, reaction of complex **5** with $AgPF_6$ in MeCN at reflux temperature gave the solvento complex **6** (Scheme 2). The reaction progress is conveniently monitored optically as the bright orange solution turns colorless upon displacement of the Cl^- and cymene ligands. The NMR spectra of complex **6** reveal only one set of signals and thus support the notion of diastereomeric mixtures in **5**. Evidently, the ruthenium centers are achiral in **6**. The carbene carbon is further deshielded (from δ_C 203 to 207.6 ppm), and also the central arene protons

undergo a slight downfield shift, δ_H 8.11 and 8.58 ppm. Three different types of MeCN ligands are resolved, with one set (δ_H 2.09 ppm) twice as intense as the other two sets (δ_H 2.60 and 1.96 ppm, respectively). These features support an octahedral coordination geometry of the ruthenium centers with two MeCN in mutual *trans* position and hence symmetry-related. Based on the stronger donor properties of NHCs *vs* pyridine ligands, the most deshielded resonance was tentatively attributed to the MeCN ligand *trans* to the pyridyl donor and the resonance at highest field to the MeCN *trans* to the carbene.

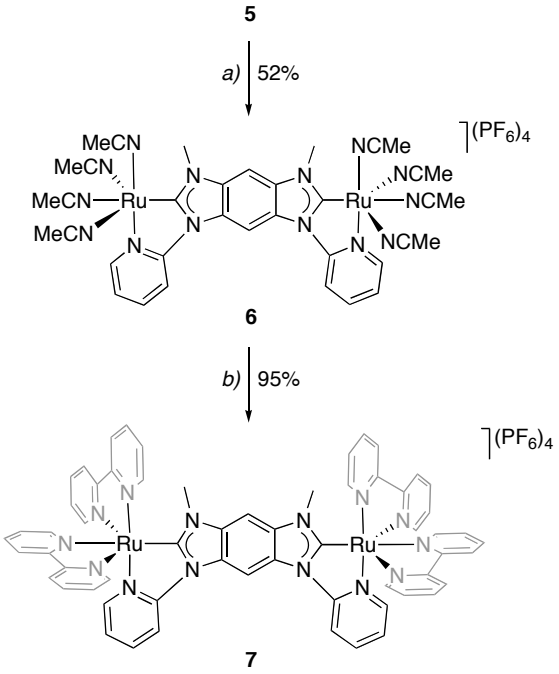

Scheme 2. Synthesis of complexes **6** and **7**. *Reagents and conditions*: a) $AgPF_6$, MeCN, reflux, 20 h; b) 2,2'-bipyridine, $MeNO_2$, reflux, 20 h.

Crystals of **6** suitable for an X-ray diffraction analysis were obtained by slow diffusion of Et_2O into a MeCN solution of the complex. The molecular structure (Fig. 2) confirms the octahedral geometry of the two ruthenium centers, with only little angular distortion. The bite angle of the *C,N*-bidentate ligand is 78.5(4)°, which is in line with related structures featuring pyridyl-substituted NHC ligands.[26] As a consequence of this acute bite angle, the overall molecular shape of **6** is curved.[27] The Ru–N bonds for the MeCN ligands *trans* to the carbenes (2.115(6) Å and 2.113(6) Å) are significantly longer than the remaining Ru–N distances (2.02–2.04 Å, Table 1). This elongation is in agreement with a substantially stronger *trans* influence of the carbene ligand, which is often correlated with its strong σ-donor ability. The metal-metal separation in **6** is 10.537(2) Å and hence some 0.2 Å shorter than the Ru…Ru distance in a bimetallic complex with an analogous ditopic ligand that lacks

chelating wingtip groups.[18] This difference is almost fully accounted for by the shorter Ru–C bond upon chelation, *viz.* 1.95(1) Å in **6** *vs* 2.065(4) Å in the monodentate analogue.

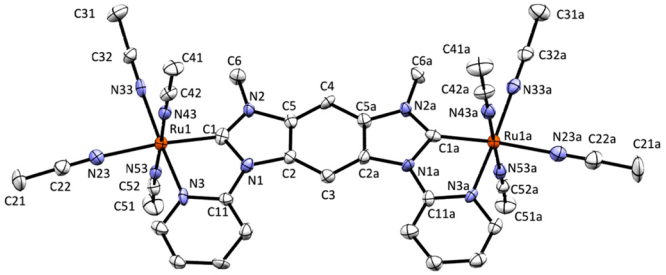

Figure 2. ORTEP view of complex **6** (50% probability ellipsoids; Hydrogen atoms, counter-ions and co-crystallized MeCN molecules omitted for clarity).

Table 2. Selected bond lengths (Å) and angles (°) for complexes **6**, and **10**.

		6 [a)]	**10**
Ru1-C1	1.955(6)	1. 945(6)	1.979(4)
Ru1-N3	2.053(6)	2.059(6)	2.068(5)
Ru1-N23	2.115(6)	2.113(6)	2.126(3)
Ru1-N33	2.042(6)	2.038(6)	2.046(6)
Ru1-N43	2.034(6)	2.025(6)	2.074(5)
Ru1-N53	2.026(6)	2.022(6)	2.062(6)
C1-N1	1.388(9)	1.393(9)	1.393(8)
C1-N2	1.346(9)	1.380(8	1.350(7)
N1-C2	1.346(9)	1.413(8)	1.416(5)
N2-C5	1.395(8)	1.368(9)	1.413(6)
N1-C1-N2	105.2(6)	105.0(6)	104.2(5)
C1-N1-C11	116.2(6)	116.7(6)	117.3(5)
C1-Ru1-N3	78.4(3)	78.5(3)	77.7(2)
C1···C1a	6.690(8)	6.690(8)	---
Ru···Ru	10.537(2)	10.537(2)	---

a) right column pertains to east end of the complex (a labels in Fig 2).

Subsequent ligand exchange with 2,2'-bipyridine (bpy) was straightforward in $MeNO_2$ and yielded bright orange complex **7** in excellent yield (90%). Introduction of bpy directly starting from the cymene complex **5** in the presence of $AgPF_6$ was less successful and afforded a mixture of compounds containing both bipyridine and MeCN ligands bound to the ruthenium center. The NMR data of complex **7** indicate the presence of two diastereoisomers, however, the congestion of the aromatic region due to the presence of two sets of 5 inequivalent pyridyl fragments did not allow proton and carbon resonances to be fully resolved and unambiguously assigned. Most diagnostic are the shielding of the pyridyl proton in α position as well as a shift of the carbene resonance to higher field (δ_C 211.1 ppm). In addition, the

chemical shift difference between the two central arene protons increases upon bpy coordination. The two resonances appear in complex **7** at δ_H 7.69 and 8.92 ppm and are thus some 1.2 ppm apart, while $\Delta\delta$ < 0.5 ppm in **6**. Again, the sensitivity of these central protons towards peripheral ligand exchange reactions suggests that electronic coupling of the metal center with these protons and hence with the center of the molecule is effective.

Synthesis of Monocarbene Complexes. For comparative purposes, analogous monometallic complexes were prepared via a route similar to the synthesis of the bimetallic complexes **5**–**7**. Thus, stirring of complex **8**[25e] at reflux temperature in MeCN in the presence of $AgPF_6$ gave the solvento complex **9** and subsequent addition of bpy yielded complex **10** as monometallic analogue of **7** (Scheme 3). Similar spectroscopic trends as deduced for the bimetallic complexes were observed. For example, the resonance of the carbene nucleus gradually shifts upfield upon introducing MeCN and subsequently bpy spectator ligands (δ_C 198.2, 204.0, and 207.9 for **8**, **9**, and **10**, respectively). Moreover, four coordinated MeCN molecules were spectroscopically identified in **9** in the 1:2:1 ratio as discussed for the bimetallic complex **6** (see above).

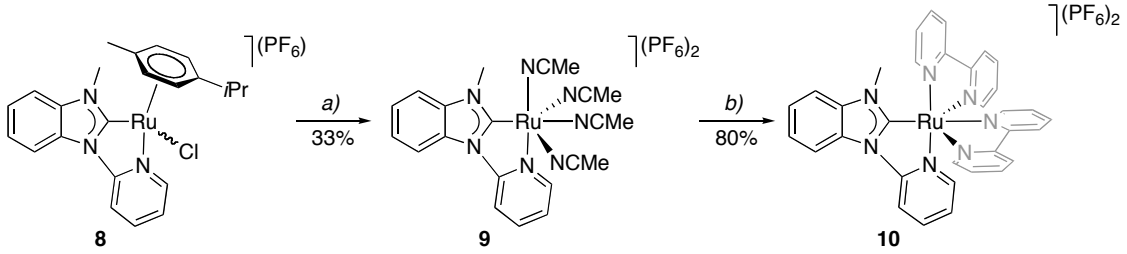

Scheme 3. Synthesis of complex **9** and **10**. *Reagents and conditions:* a) $AgPF_6$, MeCN, reflux, 20 h; b) 2,2'-bpy, $MeNO_2$, reflux, 20 h.

Crystals of **9** featured severe disorder in co-crystallized solvent molecules and PF_6^- anions, which prevented refinement to an acceptable convergence. Hence, discussion of structural data of the cationic section is limited (Fig. S2). Crystals of **10** (Fig. 3) were of better quality. The molecular structure confirms the expected connectivity pattern. The Ru–C bond (1.979(4) Å) and the Ru–$N_{pyridine}$ bond (2.068(5) Å) are slightly longer than in **6**, and consequentially, the bite angle is more acute, 77.7(2)°. As in **6** and **9**, the carbene exerts the strongest *trans* influence and the Ru–N23 bond *trans* to the NHC moiety is significantly longer (2.126(3) Å) compared to the other Ru–$N_{pyridine}$ bonds (2.046(6)–2.074(5) Å).

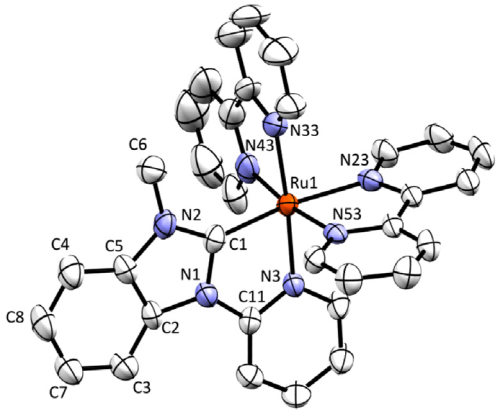

Figure 3. ORTEP view of **10** (50% probability ellipsoids; hydrogen atoms and non-coordinating PF_6^- anions omitted for clarity).

Electrochemical Analyses. Cyclovoltammetry (CV) measurements of complex **5** in CH_2Cl_2 show a single and reversible oxidation/reduction process with $E_{1/2}$ (**5**$^{2+}$/**5**) = +1.606 V *vs* SCE (Fig. S3, Table 3). This redox potential is about 0.5 V higher than that of neutral [Ru(cym)(NHC)Cl_2] complexes[18] and thus demonstrates the lower electron density in the cationic chelates, which is also reflected in the NMR deshielding of the ligand protons (see above). No further oxidation occurred up to +1.9 V. The cathodic current of the oxidation was considerably larger than the anodic current. Such behavior has previously been attributed to the adsorption of the oxidized analyte to the electrode surface.[28] In contrast, the corresponding monometallic complex **8** shows no such adsorption effect, but a similar $E_{1/2}$ (**8**$^{+}$/**8**) = +1.583 V. Differential pulse voltammetry (DPV) measurements did not show any substantial broadening of the signal recorded for **5** compared to that of the monometallic analogue **8**, indicating that the two metal centers in **5** are essentially decoupled (Class-I according to Robin and Day).[29] Measurements in MeCN or $MeNO_2$ were inconclusive and showed either an irreversible oxidation (MeCN), or no redox-process at all ($MeNO_2$). Displacement of the chloride ligand may account for the different behavior of **5** and **8** in these solvents as compared to CH_2Cl_2.

Table 3. Electrochemical data for complexes **5–10**. [a]

Complex	solvent	$E_{1/2}$ /V	ΔE /mV [b]	$\Delta E_{1/2}$ /mV	K_c [c]
5 /Ru_2	CH_2Cl_2	+1.606	151	---	---
6 /Ru_2	MeCN	+1.644, +1.888	n.d.	244	$10^{4.13}$
7 /Ru_2	CH_2Cl_2	+1.434	122	---	---
7 /Ru_2	$MeNO_2$	+1.283, +1.417	95, 95	134	$10^{2.26}$
8 /Ru	CH_2Cl_2	+1.583	116	---	---
9 /Ru	MeCN	+1.619	104	---	---
10 /Ru	CH_2Cl_2	+1.446	103	---	---

10 /Ru	$MeNO_2$	+1.287	110	---	---

a) 0.1 M $[NBu_4][PF_6]$ as supporting analyte, sweep rate 50 mV s^{-1}, potentials referenced to internal Fc^+/Fc ($E_{1/2}$ = 0.41 V), b) $\Delta E_p = E_{pa}–E_{pc}$; c) $K_c = \exp(\Delta E_{1/2}/0.059)$.

Complex **6** was measured in MeCN because its solubility in CH_2Cl_2 is low and NMR experiments showed decomposition in $MeNO_2$. A reversible redox process was observed at $E_{1/2}$ ($\mathbf{6}^{2+}/\mathbf{6}$) = +1.574 V, comparable to the monometallic model complex **9** ($E_{1/2}$ ($\mathbf{9}^{+}/\mathbf{9}$) = +1.619 V; Fig. 4). No further oxidation occurred up to +2.1 V. Compound **6** is unstable at potentials higher than +1.8 V and decomposed during electrochemical cycles, due presumably to the poor stabilization of the ruthenium(III) center by MeCN ligands. However, DPV measurements in an optically transparent thin-layer electrochemical (OTTLE) cell[30] revealed two separate processes of similar intensity which were attributed to a stepwise oxidation of the two ruthenium(II) centers with $E_{1/2}$ ($\mathbf{6}^{+}/\mathbf{6}$) = +1.644 V and $E_{1/2}$ ($\mathbf{6}^{2+}/\mathbf{6}^{+}$) = +1.888 V. These data suggest that a mixed-valence Ru^{II}/Ru^{III} state is accessible. Based on the 244 mV potential difference between the two oxidation processes and the ensuing comproportionation constant $K_c = 10^{4.13}$,[31] complex **6** corresponds to a Class II/III borderline system according to the Robin and Day classification.[29,32] These results demonstrate for the first time that efficient electronic communication of two metal centers through a rigid carbene linker is achievable. This intermetallic coupling confirms that conjugation through the benzobis(carbene) linker is effective, thus corroborating the NMR sensitivity of the central arene protons towards peripheral functionalization (*cf* NMR discussion above).

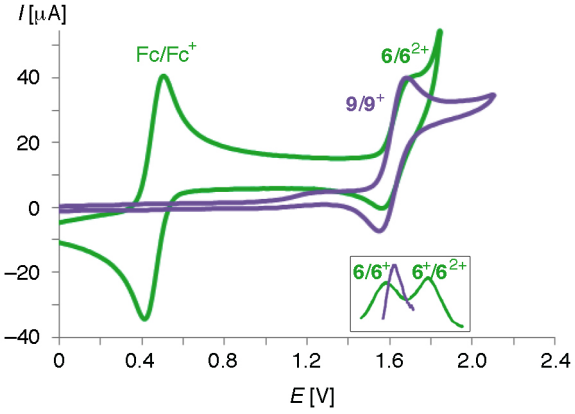

Figure 4. CV plots and relevant DPV sections (inset) of complexes **6** and **9** (1 mM in dry MeCN with 0.1 M $[NBu_4][PF_6]$ as supporting electrolyte, 50 mV s^{-1} scan rate, Fc^+/Fc used as internal standard with $E_{1/2}$ (Fc/Fc^+) = 0.41 V *vs*. SCE).

Qualitatively similar data were recorded for the bpy ligated bimetallic complex **7**. CV and DPV measurements in $MeNO_2$ show two distinct redox processes at $E_{1/2}$ ($\mathbf{7}^{+}/\mathbf{7}$) = +1.283 V

and $E_{1/2}$ ($\mathbf{7}^{2+}/\mathbf{7}^{+}$) = +1.417 V (Fig. 5). The lower oxidation potential compared to **6** underlines the stronger donor properties of bpy *vs* MeCN.[33] The stability of the oxidized species is much improved and the oxidations are fully reversible. The peak potential separation $\Delta E_{1/2}$ = 134 mV is smaller than for the acetonitrile complex **6**, yielding a comproportionation constant $K_c = 10^{2.26}$ (Class II system in the Robin and Day classification). The monometallic analogue **10** undergoes one oxidation with $E_{1/2}$ ($\mathbf{13}^{+}/\mathbf{13}$) = +1.287 V, identical to the first oxidation of **7**. When measured in CH_2Cl_2, complex **7** showed only one single redox process in CV and DPV ($E_{1/2}$ ($\mathbf{7}^{2+}/\mathbf{7}$) = +1.434 V). The asymmetric shape of the DPV signal and the large anodic peak current hint to fast decomposition in this solvent (Fig. S4).

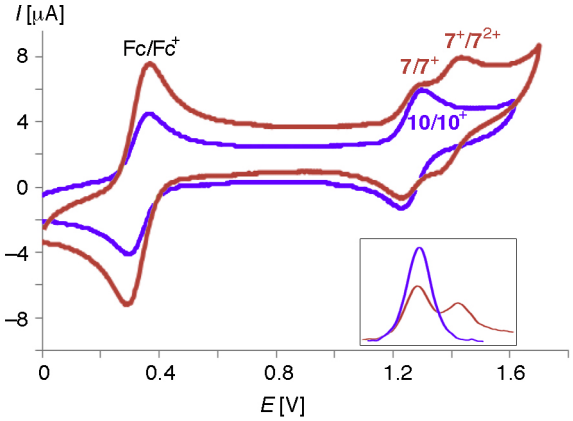

Figure 5. CV plots and relevant DPV sections (inset) of complexes **7** and **10** (1 mM in dry $MeNO_2$ with 0.1 M $[NBu_4][PF_6]$ as supporting electrolyte, 50 mV s^{-1} scan rate, Fc^+/Fc used as internal standard with $E_{1/2}$ (Fc/Fc^+) = 0.35 V *vs*. SCE).

Spectroelectrochemistry and Hush Analysis. The mixed-valent species derived from complexes **6** and **7** were further investigated by spectroelectrochemical methods using an OTTLE cell.[30,34] Complex **6** shows a strongly potential-dependent absorption behavior (Fig. 6). In the absence of an applied potential, the complex features a strong absorption band at 333 nm, tentatively assigned to a metal-to-ligand charge transfer band. At +1.37 V, the spectrum shows a markedly reduced intensity of the UV absorption and a broad absorption in the NIR region (λ_{max} = 1593 nm, ε = 13,100 $M^{-1}cm^{-1}$) that is diagnostic for an intervalence charge transfer (IVCT) and thus supports the formation of a mixed-valent Ru^{III}/Ru^{II} species $\mathbf{6}^{+}$. Further increase of the potential to +1.6 V reduces the IVCT intensity. The fully oxidized Ru^{III}/Ru^{III} species $\mathbf{6}^{2+}$ is characterized by a shallow absorption maximum at λ_{max} = 838 nm and a transparent absorption window until nearly 300 nm. Complex **7** features qualitatively identical properties , including a MLCT band at λ_{max} = 411 nm, a broad IVCT band centered

at 1652 nm (ε = 2780 $M^{-1}cm^{-1}$) upon applying a +1.23 V potential, and a weak absorption at 733 nm for the fully oxidized species $\mathbf{7}^{2+}$ at +1.5 V (Fig. S5).

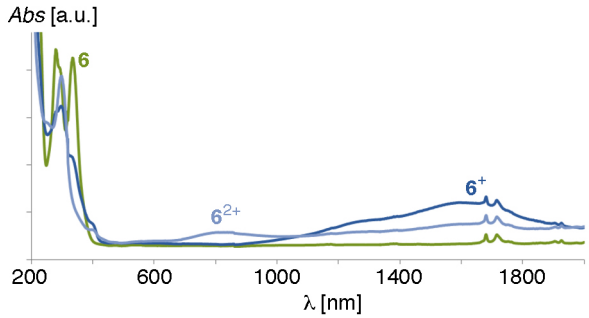

Figure 6. Absorption spectra (MeCN solutions) of complexes **6** at 0.0 V (green), $\mathbf{6}^{+}$ at +1.37 V (dark blue) and $\mathbf{6}^{2+}$ at +1.6 V (light blue).

The stability of the oxidized species was evaluated by time-dependent monitoring of the IVCT absorbance and the band around 800 nm, respectively. Thus exposing complex **6** to a potential of +1.46 V for prolonged periods of time induces a gradual decay of the absorbance at 1590 nm to about 50% within 1 h (Fig. S6). At a higher potential (+1.6 V), the decay is even faster and the absorbance at 820 nm is depleted within few minutes ($t_{1/2}$ ca. 2 min), suggesting a low stability of $\mathbf{6}^{+}$ and even a lower one for $\mathbf{6}^{2+}$. Moreover, in a CV measurement of **6** between +1.0 and +2.0 V, the IVCT absorption intensity in the anodic scan is reduced to about 20% of the absorption during the cathodic scan (Fig. 7a). These measurements thus corroborate the poor stability of oxidized $\mathbf{6}^{+}$ and $\mathbf{6}^{2+}$ as deduced from initial CV measurements (see above).

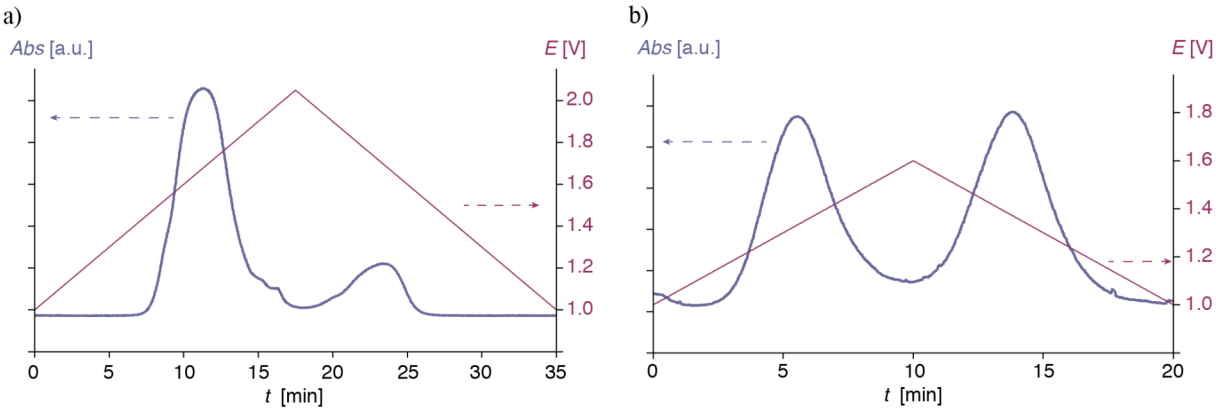

Fig 7. a) Absorbance change at 1590 nm upon a redox cycle between 1.0–2.0 V of **6** (1 mM in MeCN, 1 mV s^{-1} scan rate); b) Absorbance change at 1730 nm upon a redox cycle between 1.0–1.6 V of **7** (1 mM in $MeNO_2$, 1 mV s^{-1} scan rate).

In contrast, the bpy spectator ligands greatly enhance the stability of the oxidized forms of **7** and hence improve the reversibility substantially. For example, the decay of the IVCT absorbance band of the mixed-valent Ru^{II}/Ru^{III} species $\mathbf{7}^{+}$ is only moderate (~5% decrease

within 100 min), probably due to disproportionation. The fully oxidized Ru^{III}/Ru^{III} complex $\mathbf{7}^{2+}$ did not show any signs of degradation (Fig. S7). Moreover, the IVCT absorbance of the species at 1730 nm is equally intense in anodic and cathodic scans (Fig. 7b). These results underline the relevance of a judicious choice of spectator ligands for both stability and electronic coupling.[35]

Analysis of the IVCT bands by Marcus' theory[36] and by methods developed by Hush[5b,d] allows the degree of coupling of the metal centers to be further detailed (Table 4). The IVCT bands for $\mathbf{6}^{+}$ and $\mathbf{7}^{+}$ is considerably asymmetric (Fig. S8), with the bandwidth at half height on the high energy side, $\Delta\nu_{1/2\,(high)}$, about twice as large as that at the low energy side, $\Delta\nu_{1/2\,(low)}$. The observed bandwidth at half height $\Delta\nu_{1/2\,(obs)}$ = 2412 cm^{-1} for $\mathbf{6}^{+}$ and 2219 cm^{-1} for $\mathbf{7}^{+}$. These values are significantly smaller than the values calculated from the Hush approximation for a valence-trapped class II system ($\Delta\nu_{1/2\,(calcd)}$ 3808 cm^{-1} and 3736 cm^{-1} for $\mathbf{6}^{+}$ and $\mathbf{7}^{+}$, respectively).[5d,37] These deviations suggest a substantial degree of valence delocalization. The electronic coupling parameter H_{ab} was calculated to be 729 cm^{-1} (0.090 eV) and 377 cm^{-1} (0.047 eV), respectively.[5] The different H_{ab} values determined for $\mathbf{6}^{+}$ and $\mathbf{7}^{+}$ may potentially hint to a strong solvent dependence, which is characteristic for a class II system.[11b] However, since all further electrochemical and spectroscopic analyses point to borderline class II/III systems, we attribute this difference to a better d_M–π_L overlap in complex **6** containing weakly donating ancillary MeCN ligands, which strengthen the M–CNHC bond and hence increase the electronic coupling of the metal centers. Accordingly, the valence delocalization in $\mathbf{6}^{+}$ is more pronounced than in complex $\mathbf{7}^{+}$ containing two bpy spectator ligands. In agreement with the classification of $\mathbf{6}^{+}$ and $\mathbf{7}^{+}$ as borderline valence-trapped/delocalized mixed-valent systems, the delocalization parameter Γ is very close to 0.5.

Table 4. Spectroscopic analysis of mixed-valence complexes $\mathbf{6}^{+}$ and $\mathbf{7}^{+}$ a)

	Solvent	ν_{max}	ε_{max}	$\Delta\nu_{1/2\,(obs)}$	$\Delta\nu_{1/2\,(calcd)}$	asymmetry b)	H_{ab} c)	Γ
$\mathbf{6}^{+}$	MeCN	6277	13078	2412	3808	1.87	729 cm^{-1} (0.0904 eV)	0.37
$\mathbf{7}^{+}$	$MeNO_2$	6042	2783	2219	3736	2.06	377 cm^{-1} (0.0467 eV)	0.41

a) ν in cm^{-1}, ε in $M^{-1}cm^{-1}$; b) asymmetry of IVCT band determined as ratio $\Delta\nu_{1/2\,(high)}/\Delta\nu_{1/2\,(low)}$; c) Ru…Ru distance R = 10.537 Å from X-ray crystal structure of **6**).

Conclusions

By introducing rigidly planar chelating pyridyl wingtip groups, ditopic benzobis(carbene) ligands become effective linkers for imparting electronic coupling between two coordinated

ruthenium centers. Intermetallic communication is critically triggered by appropriate alignment of the metal 4d and the ligand π orbitals as a key principle to overcome the hitherto poor coupling in dicarbene species. Small overlap and hence insignificant Ru…Ru coupling results from coordination of the chelate to pseudo-tetrahedral metal coordination geometries as in the cymene complex **5**, and also emanates from monodentate carbene coordination, since the carbene is typically rotated out of the metal coordination plane by 30–45°. In contrast, chelation to octahedral metal centers as in **6** and **7** induces sufficiently large d_M–π_L overlap for imparting a high degree of intermetallic electronic communication, reminiscent of the poor *vs* pronounced π bonding established in pyridine and bipyridine complexes, respectively. These data lend further support to the relevance of π contributions to the metal–NHC bond.

Appropriate substitution of the ancillary ligands enhances the efficiency of the electronic communication and thus provides an opportunity for tailoring the electronic properties of the redox switch. Thus, while spectro-electrochemcial analyses indicate that both MeCN and bpy spectator ligands provide borderline class-II/III systems, valence delocalization is more pronounced in complex **6** with peripheral MeCN ligands than in complex **7** containing bpy spectator ligands. Besides affecting the stability of the different oxidation states and the reversibility of the redox processes, spectator ligands thus also influence the degree of communication. This relevance needs to be taken into account when designing a next generation of molecular switches based on the bis(carbene) synthon.

Our results provide unambiguous evidence that N-heterocyclic carbene-based ligands are suitable linkers for the fabrication of molecular redox switches. They constitute synthetically versatile alternatives to the more popular oligopyridine- and alkyne-derived linkers, thus offering to novel synthons for application in organometallic polymer chemistry, in molecular electronics, and potentially also in computing.

Experimental Section

General comments. Starting materials were commercially available and used as received. Solvents were purified using a Thermovac alumina/catalyst column system. The synthesis of complexes **8** and **10** was described previously.[25e] Where indicated, reactions were conducted in a Biotage Initiator Microwave Synthesizer. ^{1}H and ^{13}C{^{1}H} NMR spectra were recorded with Bruker spectrometers at RT unless stated otherwise. Chemical shifts (δ) are given in ppm relative to signals of residual protio solvent (coupling constants J in Hz). Signals were

assigned with the aid of two-dimensional cross-coupling experiments. Elemental analyses were performed by the Microanalytical Laboratory of the ETH Zürich (Switzerland).

Electrochemistry. Electrochemical studies were carried out using an EG&G Princeton Applied Research Potentiostat, Model 273A, employing a gas-tight three electrode cell under an argon atmosphere. A glassy carbon disk with 3.41 mm^2 surface area was used as the working electrode and was polished before each measurement. The reference electrode was Ag/AgCl and the counter electrode was a Pt wire. In all experiments, Bu_4NPF_6 (0.1 M in dry solvent) was used as supporting electrolyte with analyte concentrations of approximately 1 mM. Measurements were performed at different scan rates (50–250 mV s^{-1}). All redox potentials were referenced to the ferrocenium/ferrocene couple (Fc^+/Fc) as internal standard with $E_{1/2}$ (Fc^+/Fc) *vs*. SCE = +0.46 V in CH_2Cl_2, +0.40 V in MeCN, +0.35 V in $MeNO_2$.[38] Spectroelectrochemical studies were performed using an EG&G Princeton Applied Research Potentiostat, Model 273A and a Perkin Elmer UV-Vis-NIR Spectrometer, Model Lambda 900, employing an optically transparent thin-layer electrochemical (OTTLE) cell.[30] In all experiments, Bu_4NPF_6 (0.1 M in MeCN or $MeNO_2$) was used as supporting electrolyte with analyte concentrations of approximately 1 mM. For Hush analysis,[5] data were first treated to remove solvent artifacts by subtracting the absorbance at ground potential, assuming that there is no relevant absorbance in the NIR region but background and solvent. The baseline was corrected and absorbance values were smoothened over 9 data points. The IVCT band of $\mathbf{6}^+$ (ν_{max} = 6277 cm^{-1}) contains a shoulder towards high energy. Assuming that the shoulder arises from a minor decomposition product, it was removed by curve fitting. Transformation from absorbance to molar extinction ε was calculated *via* Beer-Lambert law (1 mM concentrations, path length d = 0.2 mm for the OTTLE cell). Integrals were calculated numerically and yielded induced dipole moment μ_{ge} = 7.31 D for $\mathbf{6}^+$ and 3.16 D for $\mathbf{7}^+$ according to Eq. 1

$$\mu_{ge} = 0.09584\ (\int \varepsilon(\nu) \partial \nu\ /\ \nu_{max})^{1/2} \quad (1)$$

The electronic coupling was calculated according to Eq. 2

$$H_{ab} = \mu_{ge} \times \nu_{max} / (e \times R) \quad (2)$$

with R taken from the Ru…Ru distance in **6** as determined by X-ray crystallography (10.537 Å) and is the elementary charge. The delocalization parameter Γ was calculated according to Eq. 3

$$\Gamma = 1 - (\nu_{1/2\ (obs)} / \nu_{1/2\ (calcd)}) \quad (3)$$

with $\nu_{1/2\,(calcd)} = (2310 \times \nu_{max})^{1/2}$.

Synthesis of 1. 1,5-Dichloro-2,4-dinitrobenzene (2.76 g, 11.6 mmol) and 2-aminopyridine (24.0 g, 255 mmol) were stirred neat at 90°C for 3 d. The mixture was poured into MeCN (50 mL) and water was added until a yellow precipitate formed. This precipitate was isolated by filtration and dried in vacuo to yield **1** as an analytically pure yellow solid (3.59 g, 87%). ^{1}H NMR (360 MHz $CDCl_3$): δ = 10.64 (br s, 2H, NH), 10.26 (s, 1H, H_{Ar}), 9.38 (s, 1H, H_{Ar}), 8.44 (d, $^{3}J_{HH}$ = 4.5 Hz, 2H, H_{py}), 7.75 (t, $^{3}J_{HH}$ = 8.0 Hz, 2H, H_{py}), 7.17 (d, $^{3}J_{HH}$ = 8.0 Hz, 2H, H_{py}), 7.09 (dd, $^{3}J_{HH}$ = 4.5 Hz, $^{3}J_{HH}$ = 8.0 Hz, 2H, H_{py}). $^{13}C\{^{1}H\}$ NMR (75 MHz, $CDCl_3$): δ = 152.5 (C_{py}–C), 148.1 (C_{py}–H), 143.4 (C_{Ar}–NO_2), 138.2 (C_{py}–H), 127.9 (C_{Ar}–H), 126.6 (C_{Ar}–NH), 119.3 (C_{py}–H), 114.9 (C_{py}–H), 103.4 (C_{Ar}–H). Elem. Anal. Calcd for $C_{16}H_{12}N_6O_4$ (352.31): C 54.55, H 3.43, N 23.84%; Found C 54.71, H 3.52, N 23.88%.

Synthesis of 2. Compound **1** (800 mg, 2.3 mmol) was dissolved in a mixture of $HC(OEt)_3$ (26 mL) and HCOOH (85%, 2.2 mL, 58 mmol) under argon atmosphere. Sodium formate (3.56 g, 52 mmol) and Pd/C 10% (0.6 mg, 0.52 mmol) were added and the reaction was stirred at 100 °C for 36 h. After cooling, the reaction mixture was filtered and the filtrate treated with aqueous HCl (6%) and stirred for 10 min. The yellow solution was treated with aqueous NaOH (10%) until basic and allowed to stand for 1 h. The resulting solid was collected by filtration, washed with H_2O and dried to yield crude **2** (567 mg, 81%). Recrystallization from CH_2Cl_2/pentane mixture afforded an analytically pure sample. ^{1}H NMR (300 MHz $CDCl_3$): δ = 8.92 (s, 1H, H_{Ar}), 8.66 (dd, $^{3}J_{HH}$ = 4.8 Hz, $^{4}J_{HH}$ = 1.5 Hz,2H, H_{py}), 8.62 (s, 2H, NCHN), 8.32 (s, 1H, H_{Ar}), 7.95 (td, $^{3}J_{HH}$ = 8.1 Hz, $^{4}J_{HH}$ = 1.5 Hz, 2H, H_{py}), 7.65 (d, $^{3}J_{HH}$ = 8.1 Hz, 2H, H_{py}), 7.33 (dd, $^{3}J_{HH}$ = 8.1 Hz, $^{3}J_{HH}$ = 4.9 Hz, 2H, H_{py}). $^{13}C\{^{1}H\}$ NMR (75 MHz, $CDCl_3$): δ = 150.3 (C_{py}–C), 149.5 (C_{py}–H), 142.2 (NCHN), 142.2 (C_{Ar}–N), 139.0 (C_{py}–H), 130.6 (C_{Ar}–N), 121.6 (C_{py}–H), 114.2 (C_{py}–H), 111.0 (C_{Ar}–H), 96.2 (C_{Ar}–H). Elem. Anal. Calcd for $C_{18}H_{12}N_6$ (312.33) × 1/8 CH_2Cl_2: C 67.41, H 3.82, N 26.02%; Found: C 67.78, H 4.10, N 25.61%.

Synthesis of 3. Compound **2** (567 mg, 1.8 mmol) was suspended in a mixture of MeI (2.0 mL, 32 mmol) and MeCN (0.1 mL). The reaction mixture was sealed in a pressure tube and heated to 110 °C for 48 h. After cooling the reaction mixture was filtered and the residue was washed with a minimum amount of MeCN and Et_2O and dried in vacuo, yielding **3** as analytically pure and slightly hygroscopic off-white powder (569 mg, 52%). ^{1}H NMR (400

MHz, DMSO–d_6): δ = 10.84 (s, 2H, NCHN), 9.65 (s, 1H, H_{Ar}), 9.13 (s, 1H, H_{Ar}), 8.85 (d, $^3J_{HH}$ = 4.5 Hz, 2H, H_{py}), 8.36 (t, $^3J_{HH}$ = 8.0 Hz, 2H, H_{py}), 7.65 (d, $^3J_{HH}$ = 8.0 Hz, 2H, H_{py}), 7.33 (dd, 2H, $^3J_{HH}$ = 8.0 Hz, $^3J_{HH}$ = 4.5 Hz, 2H, H_{py}), 4.33 (s, 6H, N–CH_3). $^{13}C\{^1H\}$ NMR (100 MHz, DMSO–d_6): δ = 149.4 (C_{py}–C), 147.5 (C_{py}–H), 146.6 (NCHN), 140.8 (C_{py}–H), 131.4 (C_{Ar}–N), 128.5 (C_{Ar}–N), 125.2 (C_{py}–H), 116.8 (C_{py}–H), 103.6 (C_{Ar}–H), 99.7 (C_{Ar}–H), 34.5 (N–CH_3). Elem. Anal. Calcd for $C_{20}H_{18}I_2N_6$ (596.21) × 1/2 H_2O: C 39.69, H 3.16, N 13.89%; Found: C 39.57, H 3.26, N 13.82%.

Synthesis of 4. Compound **3** (569 mg, 1.0 mmol) was dissolved in H_2O (80 mL) and a solution of $(NH_4)PF_6$ (3.23 g, 20 mmol) in H_2O (10 mL) was added under vigorous stirring. The formed precipitate was collected by filtration and dried in vacuo to yield **4** as analytically pure white powder (502 mg, 87%). ^1H NMR (360 MHz, DMSO–d_6): δ = 10.80 (s, 2H, NCHN), 9.65 (s, 1H, H_{Ar}), 9.08 (s, 1H, H_{Ar}), 8.85 (d, $^3J_{HH}$ = 4.1 Hz, 2H, H_{py}), 8.35 (t, $^3J_{HH}$ = 8.0 Hz, 2H, H_{py}), 8.10 (d, $^3J_{HH}$ = 8.0 Hz, 2H, H_{py}), 7.77 (dd, $^3J_{HH}$ = 8.0 Hz, $^3J_{HH}$ = 4.1 Hz, 2H, H_{py}), 4.32 (s, 6H, N–CH_3). $^{13}C\{^1H\}$ NMR (90 MHz, DMSO–d_6): δ = 149.7 (C_{py}–C), 147.6 (C_{py}–H), 146.7 (NCHN), 140.9 (C_{py}–H), 131.5 (C_{Ar}–N), 128.6 (C_{Ar}–N), 125.4 (C_{py}–H), 116.8 (C_{py}–H), 103.5 (C_{Ar}–H), 99.7 (C_{Ar}–H), 34.5 (N–CH_3). Elem. Anal. Calcd for $C_{20}H_{18}F_{12}N_6P_2$ (632.33): C 37.99, H 2.87, N 13.29%; Found C 38.12, H 3.06, N 13.24%.

Synthesis of complex 5. To a suspension of benzobisimidazolium salt **4** (100 mg, 0.16 mmol) in MeOH (10 mL) was added Ag_2O (81 mg, 0.35 mmol). The reaction mixture was stirred in the dark under argon at RT for 24 h. All volatiles were evaporated and the residue was suspended in dry CH_2Cl_2 (10 mL). After addition of $[RuCl_2(p\text{-cymene})]_2$ (106.4 mg, 0.17 mmol), the suspension was stirred at RT for 72 h protected from light. The mixture was then centrifuged and the supernatant was decanted and filtered through a short pad of Al_2O_3. After evaporation and drying in vacuo, complex **5** was obtained as an orange solid in a 1:1 mixture of diastereomers (167 mg, 90%). ^1H NMR (400 MHz $CDCl_3$), *isomer A*: δ = 9.27 (d, $^3J_{HH}$ = 5.2 Hz, 2H, H_{py}), 7.90–7.96 (m, 4H, H_{py}), 7.84 (s, 1H, H_{Ar}), 7.69 (s, 1H, H_{Ar}), 7.49–7.56 (m, 2H, H_{py}), 6.37 (d, $^3J_{HH}$ = 6.3 Hz, 2H, H_{cym}), 6.23 (d, $^3J_{HH}$ = 6.3 Hz, 2H, H_{cym}), 6.14 (d, $^3J_{HH}$ = 6.5 Hz, 2H, H_{cym}), 5.78 (d, $^3J_{HH}$ = 6.5 Hz, 2H, H_{cym}), 3.98 (s, 6H, N–CH_3), 2.38 (septet, $^3J_{HH}$ = 6.6 Hz, 2H, $CHMe_2$), 2.28 (s, 6H, cym–CH_3), 0.92 (d, $^3J_{HH}$ = 6.6 Hz, 6H, CH–CH_3), 0.83 (d, $^3J_{HH}$ = 6.6 Hz, 6H, CH–CH_3). *Isomer B*: δ = 9.30 (d, $^3J_{HH}$ = 5.6 Hz, 2H, H_{py}), 8.56 (s, 1H, H_{Ar}), 8.45 (d, $^3J_{HH}$ = 8.3 Hz, 2H, H_{py}), 8.33 (t, $^3J_{HH}$ = 8.0 Hz, 2H, H_{py}), 8.20 (s, 1H, H_{Ar}), 7.56

(t, $^3J_{HH}$ = 6.3 Hz, 2H, H_{py}), 6.31 (d, $^3J_{HH}$ = 6.3 Hz, 2H, H_{cym}), 6.28 (d, $^3J_{HH}$ = 6.3 Hz, 2H, H_{cym}), 6.05 (d, $^3J_{HH}$ = 6.5 Hz, 2H, H_{cym}), 5.72 (d, $^3J_{HH}$ = 6.5 Hz, 2H, H_{cym}), 4.43 (s, 6H, N–CH_3), 2.46 (septet, $^3J_{HH}$ = 6.6 Hz, 2H, $CHMe_2$), 2.22 (s, 6H, cym–CH_3), 0.92 (d, $^3J_{HH}$ = 6.6 Hz, 6H, CH–CH_3), 0.83 (d, $^3J_{HH}$ = 6.6 Hz, 6H, CH–CH_3). $^{13}C\{^1H\}$ NMR (100 MHz $CDCl_3$), *isomer A:* 202.8 (C–Ru), 154.4 (C_{py}–C), 153.0 (C_{py}–H), 143.4 (C_{py}–H), 135.7 (C_{Ar}–N), 127.8 (C_{Ar}–N), 125.0 (C_{py}–H), 115.1 (C_{py}–H), 111.7 (C_{cym}–C), 108.4 (C_{cym}–C), 96.7 (C_{Ar}–H), 95.9 (C_{Ar}–H), 94.3 (C_{cym}–H), 92.9 (C_{cym}–H), 89.5 (C_{cym}–H), 85.2 (C_{cym}–H), 37.4 (N–CH_3), 32.1 ($CHMe_2$), 22.7 (CH–CH_3), 22.5 (C–CH_3), 19.6 (cym–CH_3). *Isomer B*: δ = 203.3 (C–Ru),157.4 (C_{py}–C), 153.0 (C_{py}–H), 142.9 (C_{py}–H), 134.5 (C_{Ar}–N), 128.8 (C_{Ar}–N), 124.3 (C_{py}–H), 114.9 (C_{py}–H), 111.2 (C_{cym}–C), 108.4 (C_{cym}–C), 97.8 (C_{Ar}–H), 95.9 (C_{Ar}–H), 94.3 (C_{cym}–H), 94.0 (C_{cym}–H), 89.3 (C_{cym}–H), 85.4 (C_{cym}–H), 37.5 (N–CH_3), 32.1 ($CHMe_2$), 22.6 (C–CH_3), 22.5 (C–CH_3), 19.4 (cym–CH_3). Elem. Anal. Calcd for $C_{40}H_{42}Cl_2F_{12}N_6P_2Ru_2$ (1171.79) × CH_2Cl_2: C 39.18, H 3.69, N 6.69%; Found C 38.98, H 3.90, N 6.97%.

Synthesis of complex 6. Complex **5** (140 mg, 0.12 mmol) was dissolved in MeCN (10 mL) and $AgPF_6$ (121 mg, 0.48 mmol) was added. The mixture was heated to reflux and stirred for 20 h. After cooling, the reaction mixture was poured into H_2O (10 mL). The formed precipitate was filtered, washed with Et_2O (3 × 5 mL) and dried to yield analytically pure complex **6** as an off-white powder (91 g, 52%). X-ray quality crystals were grown by slow diffusion of Et_2O into a MeCN solution of **6** at –20 °C. ^1H NMR (400 MHz, $CDCl_3$): δ = 9.05 (d, $^3J_{HH}$ = 5.7 Hz, 2H, H_{py}), 8.58 (s, 1H, H_{Ar}), 8.48 (d, $^3J_{HH}$ = 8.2 Hz, 2H, H_{py}), 8.33 (t, $^3J_{HH}$ = 8.2 Hz, 2H, H_{py}), 8.11 (s, 1H, H_{Ar}), 7.56 (dd, $^3J_{HH}$ = 8.2 Hz, $^3J_{HH}$ = 5.7 Hz, 2H, H_{py}), 4.41 (s, 6H, N–CH_3), 2.60 (s, 6H, $NCCH_3$), 2.09 (s, 12H, $NCCH_3$), 1.96 (s, 6H, $NCCH_3$). $^{13}C\{^1H\}$ NMR (100 MHz, $CDCl_3$): δ = 207.6 (C–Ru), 156.4 (C_{py}–C), 154.7 (C_{py}–H), 142.2 (C_{py}–H), 136.0 (C_{Ar}–N), 129.9 (C_{Ar}–N), 127.9 (NCMe), 126.2 (NCMe), 125.4 (NCMe), 123.4 (C_{py}–H), 114.3 (C_{py}–H), 95.9 (C_{Ar}–H), 94.8 (C_{Ar}–H), 37.9 (N–CH_3), 4.9 (NC–CH_3), 4.4 (NC–CH_3), 1.1 (NC–CH_3). Elem. Anal. Calcd for $C_{36}H_{40}F_{24}N_{14}P_4Ru_2$ (1452.02): C 29.80, H 2.78, N 13.52%; Found C 29.67, H 2.89, N 13.30%.

Synthesis of complex 7. A pressure tube was charged with complex **6** (60 mg, 41 μmol), 2,2-bipyridine (60 mg, 0.38 mmol) and $MeNO_2$ (4 mL) and stirred at 110 °C for 20 h. After cooling, the orange reaction mixture was poured into Et_2O (20 mL) and the formed precipitate was filtered off, washed with Et_2O and dried to give complex **7** as an orange solid (86 mg,

95%). Recrystallization from CH_2Cl_2/pentane gave an analytically pure sample and crystals suitable for an X-ray diffraction analysis. NMR spectroscopy revealed a 1:1 mixture of two diastereomers. ^{1}H NMR (500 MHz, $CDCl_3$): δ = 8.92 (s, 2H, H_{Ar}), 8.64 (d, 4H, H_{bpy}), 8.63 (d, 4H, H_{bpy}), 8.62 (d, 2H, H_{py}), 8.61 (d, 2H, H_{bpy}), 8.59 (d, 2H, H_{py}'), 8.56 (d, 2H, H_{bpy}), 8.55 (d, 2H, H_{bpy}), 8.53 (d, 2H, H_{bpy}), 8.26 (t, 4H, H_{bpy}), 8.24 (d, 2H, H_{py}), 8.21 (t, 4H, H_{bpy}), 8.20 (d, 2H, H_{py}'), 8.15 (t, 2H, H_{bpy}), 8.12 (t, 2H, H_{bpy}), 8.10 (t, 2H, H_{bpy}), 8.09 (t, 2H, H_{bpy}), 8.09 (t, 2H, H_{py}), 8.06 (t, 2H, H_{py}'), 8.00 (d, 2H, H_{bpy}), 7.98 (d, 2H, H_{bpy}), 7.86 (t, 4H, H_{bpy}), 7.85 (d, 2H, H_{bpy}), 7.80 (t, 4H, H_{bpy}), 7.79, (d, 2H, H_{bpy}), 7.69 (s, 2H, H_{Ar}), 7.58 (dd, 4H, H_{bpy}), 7.45 (dd, 2H, H_{bpy}), 7.44 (dd, 2H, H_{bpy}), 7.42 (dd, 2H, H_{bpy}), 7.41 (dd, 2H, H_{bpy}), 7.40 (dd, 2H, H_{py}), 7.31 (dd, 4H, H_{bpy}), 7.30 (dd, 2H, H_{py}'), 3.50 (s, 12H, N–CH_3). ^{13}C{^{1}H} NMR (125 MHz, $CDCl_3$): δ = 211.1 (C–Ru), 158.3–156.2 (C^2_{py}), 156.7–150.3 (C^3_{py}), 141.5–139.2 (C^4_{py}), 136.7 (C_{Ar}–N), 130.3 (C_{Ar}–N), 130.3–124.1 (C^5_{py}), 125.9–114.4 (C^6_{py}), 96.2 (C_{Ar}–H), 93.7 (C_{Ar}–H), 34.0 (N–CH_3). Elem. Anal. Calcd for $C_{60}H_{48}F_{24}N_{14}P_4Ru_2$ (1747.11): C 41.25, H 2.77, N 11.22%; Found C 40.96, H 3.21, N 11.01%.

Synthesis of complex 9. Complex **8** (50 mg, 80 μmol) was dissolved in MeCN (8 mL) and $AgPF_6$ (45 mg, 0.18 mmol) was added. The reaction mixture was stirred at reflux temperature for 20 h. After cooling, all volatiles were evaporated and the residue was dissolved in a minimum amount of H_2O and extracted with CH_2Cl_2 (3 × 5 mL). The combined organic layers were washed with H_2O (5 mL) and dried over Mg_2SO_4. The solution was poured into pentane (30 mL) and the formed precipitate was filtered and washed with pentane. After drying in vacuo complex **9** was obtained as an off-white solid (45 mg, 33%). X-ray quality crystals were grown by slow diffusion of Et_2O into a MeCN solution of complex **9** at –20 °C. Elem. Anal. Calcd for $C_{21}H_{23}F_{12}N_7P_2Ru$ (764.45): C 32.99, H 3.03, N 12.83%; Found: C 33.23, H 2.91, N 13.04. ^{1}H NMR (300 MHz, $CDCl_3$): δ = 8.97 (dd, $^3J_{HH}$ = 5.8 Hz, $^4J_{HH}$ = 0.9 Hz, 1H, H_{py}), 8.27–8.13 (m, 3H, H_{Ar} + 2H_{py}), 7.81–7.73 (m, 1H, H_{Ar}), 7.64–7.51 (m, 2H, H_{Ar}), 7.47 (ddd, $^3J_{HH}$ = 7.2 Hz, $^3J_{HH}$ = 5.8 Hz, $^3J_{HH}$ = 1.3 Hz, 1H, H_{py}), 4.26 (s, 3H, N–CH_3), 2.56 (s, 3H, NC–CH_3), 2.07 (s, 6H, NC–CH_3), 1.96 (s, 3H, NC–CH_3). ^{13}C{^{1}H} NMR (100 MHz, $CDCl_3$): δ = 204.0 (C–Ru), 156.9 (C_{py}–C), 154.4 (C_{py}–H), 141.9 (C_{py}–H), 138.2 (C_{Ar}–N), 132.7 (C_{Ar}–N), 127.7 (NCMe), 126.1 (C_{Ar}–H), 123.0 (C_{Ar}–H), 125.1 (NCMe), 123.0 (C_{py}–H), 118.7 (NCMe), 113.7 (C_{py}–H), 112.9 (C_{Ar}–H), 112.3 (C_{Ar}–H), 35.3 (N–CH_3), 4.8 (NC–*C*H_3), 4.4 (NC–*C*H_3), 1.4 (NC–*C*H_3). Elem. Anal. Calcd for $C_{21}H_{23}F_{12}N_7P_2Ru$ (764.45): C 32.99, H 3.03, N 12.83%; Found C 33.23, H 2.91, N 13.04%.

Crystal Structure Determinations. Suitable single crystals were mounted on a StoeMark II-Imaging Plate Diffractometer System (Stoe & Cie, 2002) equipped with a graphite-monochromator. Data collection was performed using Mo-Kα radiation (λ = 0.71073 Å) with a nominal crystal to detector distance of 135 mm. All structures were solved by direct methods using SHELXS-97 and refined by full matrix least-squares on F^2 for all data using SHELXL-97.[39] The hydrogen atoms were included in calculated positions and treated as riding atoms using SHELXL-97 default parameters. Anisotropic thermal displacement parameters were used for all non-hydrogen atoms. Four independent molecules and eight disordered PF_6^- anions are present in the unit-cell of **9**. Attempts to resolve the disorder of the PF_6^- ions and solvent molecules using the SQUEEZE routine[40] were unsuccessful due to the low quality of the data. Further crystallographic details are compiled in the supporting information. CCDC numbers 949564 (**2**), 949565 (**6**), and 949566 (**10**) contain the supplementary crystallographic data for this paper. These data can be obtained free of charge from the Cambridge Crystallographic Data Centre via www.ccdc.cam.ac.uk/data_request/cif.

Acknowledgements

We thank P. Belser for fruitful discussions. This work was financially supported by a Marie Curie Intra-European Fellowship (PIEF-221323) and by the Eureopean Research Council (ERC StG-208561).

Supporting Information

Crystallographic details, ORTEP of complex **2**, electrochemical details of complexes **5–10**.

References

[1] (a) M. Irie, *Chem. Rev.* **2000**, *100*, 1683–1684. (b) S. A. Wolf, D. D. Awschalom, R. A. Buhrman, J. M. Daughton, S. von Molnar, M. L. Roukes, A. Y. Chtchelkanova, D. M. Treger, *Science* **2001**, *294*, 1488–1495. (c) J. E. Green, J. W. Choi, A. Boukai, Y. Bunimovich, . Johnston-Halperin, E. Delonno, Y. Luo, B. A. Sheriff, K. Xu, Y. S. Shin, H.-R. Tseng, J. F. Stoddart, J. R. Heath, *Nature* **2007**, *445*, 414–417. (d) J. P. Sauvage (Ed.) *Molecular Machines and Motors* , Springer (Berlin, Germany), 2001. (e) B. L. Feringa, W. R. Browne (Eds.) *Molecular Switches*, Wiley-VCH (Weinheim, Germany), 2011.

[2] (a) R. A. Bissell, E. Cordova, A. E. Kaifer, J. F. Stoddart, *Nature* **1994**, *369*, 133–137. (b) D. Astruc, *Acc. Chem. Res.* **1997**, *30*, 383–391. (c) J. M. Tour, *Acc. Chem. Res.* **2000**, *33*,

791–804. (d) D. N. Hendrickson, C. G. Pierpont, *Top. Curr. Chem.* **2004**, *234*, 63–95. (e) W. E. Geiger, *Organometallics* **2011**, *30*, 28–31.

[3] (a) O. Kahn, C. J. Martinez, *Science,* **1998**, *279*, 44–48. (b) J.-F. Létard, *Top. Curr. Chem.* **2004**, *235*, 221–249. (c) M. A. Halcrow, *Chem. Soc. Rev.* **2011**, *40*, 4119. (d) S. Venkataramani, U. Jana, M. Dommaschk, F. D. Sönnichsen, F. Tuczek, R. Herges, *Science* **2011**, *331*, 445–448.

[4] (a) S. Shinkai, T. Nakaji, Y. Nishida, T. Ogawa, O. Manabe, *J. Am. Chem. Soc.* **1980**, *102*, 5860–5865. (b) M. Irie, *Chem. Rev.* **2000**, *100*, 1685–1716. (c) B. L. Feringa, R: A. van Delden, N. Koumura, E. M. Geertsema, *Chem. Rev.* **2000**, *100*, 1789–1816. (d) V. Balzani, A. Credi, M. Venturi, *Proc. Natl. Acad. Sci. USA,* **2002**, *99*, 4814. (e) A. P. de Silva, M. R. James, B. O. F. McKinney, D. A. Pears, S. M. Weir, *Nature Mater.* **2006**, *5*, 787.

[5] (a) C. Creutz, H. Taube, *J. Am. Chem. Soc.* **1969**, *91*, 3988–3989. (b) N. S. Hush, *Prog. Inorg. Chem.* **1967**, *8*, 391–444. (c) H. Taube, *Angew. Chem. Int. Ed. Engl.* **1984**, *23*, 329. (d) N. S. Hush, *Coord. Chem. Rev.* **1985**, *64*, 135–157. (e) C. Creutz, M. D. Newton, N. Sutin, *J. Photochem. Photobiol. A,* **1994**, *82*, 47. (f) B. S. Brunschwig, C. Creutz, N. Sutin, *Chem. Soc. Rev.* **2002**, *31*, 168.

[6] (a) W. Kaim, A. Klein, M. Glöckle, *Acc. Chem. Res.* **2000**, *33*, 755. (b) J.-P. Launay, *Chem. Soc. Rev*. **2001**, *30*, 386. (c) D. M. D'Alessandro, F. R. Keene, *Chem. Rev.* **2006**, *106*, 2270. (d) W. Kaim, G. K. Lahiri, *Angew. Chem. Int. Ed.* **2007**, *46*, 1778. (e) M. H. Chisholm, N. J. Patmore, *Acc. Chem. Res.* **2007**, *40*, 19. (f) J. Hankache, O. S. Wenger, *Chem. Rev.* **2011**, *111*, 5138.

[7] (a) Aviram, A. Ratner, M. *Chem. Phys. Lett.* **1974**, *29*, 277. (b) Joachim, C. Gimzewski, J. K. Aviram, A. *Nature* **2000**, *408*, 541. (c) M. Mayor, H. B. Weber, *Angew. Chem. Int. Ed.* **2004**, *43*, 2882–2884. (d) Lindsay, S. M. Ratner, M. A. *Adv. Mater.* **2007**, *19*, 23.

[8] (a) I. Manners, *Chem. Rev.* **1999**, *99*, 1515. B. (b) J. Holliday, T. M. Swager, *Chem. Commun.* **2005**, 23. (c) J. Roncali, *J. Mater. Chem.* **1999**, *9*, 1875. (d) M. S. Gudiksen, L. J. Lauhon, J. Wang, D. C. Smith, C. M. Lieber, *Nature* **2002**, *415*, 617–620. (e) C. Moorlag, B. C. Sih, T. L. Stott, M. O. Wolf, *J. Mater. Chem.* **2005**, *15*, 33. (f) K. A. Williams, A. J. Boydston, C. W. Bielawski, *Chem. Soc. Rev.* **2007**, *36*, 729–744.

[9] P. Aguirre-Etcheverry, D. O'Hare, *Chem. Rev.* **2010**, *110*, 4839–4864.

[10] For selected representative examples, see: (a) C. Patoux, J.-P. Launay, M. Beley, S. Chodorowski-Kimmes, J.-P. Collin, S. James, J.-P. Sauvage, *J. Am. Chem. Soc.* **1998**, *120*, 3717. (b) P. Steenwinkel, D. M. Grove, N. Veldman, A. L. Spek, G. van Koten, *Organometallics* **1998**, *17*, 5647. (c) M. D. Ward, *J. Chem. Educ.* **2001**, *78*, 321. (d) S. Fraysse, C. Coudret, J.-P. Launay, *J. Am. Chem. Soc.* **2003**, *125*, 5880. (e) L. Cola, (Ed.), *Top. Curr. Chem.* **2005**, *257*. (f) A. Nitzan, M. A. Ratner, *Science* **2007**, *300*, 1384. (g) O. S. Wenger, *Coord. Chem. Rev.* **2009**, *253*, 1439. (h) N. Chanda, B. Sarkar, F. Jan, W. Kaim, G. K. Lahiri, *Dalton Trans.* **2003**, 3550–3555.

[11] (a) N. Le Narvor, L. Toupet, C. Lapinte, *J. Am. Chem. Soc.* **1995**, *117*, 7129–7138. (b) S. Barlow, D. O'Hare, *Chem. Rev.* **1997**, *97*, 637–670. (c) F. Paul, C. Lapinte, *Coord. Chem. Rev.* **1998**, *178–180*, 431–509.S. (d) Szafert, J. A. Gladysz, *Chem. Rev.* **2003**, *103*, 4175. (e) D. A. Valyaev, O. S. Semeikin, N. A. Ustynyuk, *Coord. Chem. Rev.* **2004**, *248*, 1679–1692.

[12] (a) R. Breslow, *J. Am. Chem. Soc.* **1958**, *80*, 3719–3736. (b) H. W. Wanzlick, H. J. Schönherr, *Angew. Chem. Int. Ed*. **1968**, *7*, 141. (c) K. Öfele, *J. Organomet. Chem.* **1968**, *12*, P42-P43. A. (d) A. Igau, H. Grützmacher, A. Baceiredo, G. Bertrand, *J. Am. Chem. Soc.* **1988**, *110*, 6463–6466. (e) A. J. Arduengo, R. L. Harlow, M. Kline, *J. Am. Chem. Soc.* **1991**, *113*, 361–363.

[13] (a) D. Bourissou, O. Guerret, F. P. Gabbaï, G. Bertrand, *Chem. Rev.* **2000**, *100*, 39–92. (b) F. E. Hahn, M. C. Jahnke, *Angew. Chem. Int. Ed.* **2008**, *47*, 3122–3172. (c) M. Poyatos, J. A. Mata, E. Peris, *Chem. Rev.* **2009**, *109*, 3677–3707. (d) M. Melaimi, M. Soleilhavoup, G. Bertrand, *Angew. Chem. Int. Ed.* **2010**, *49*, 8810–8849.

[14] For representative work see: (a) D. S. McGuinness, N. Saendig, B. F. Yates, K. J. Cavell, *J. Am. Chem. Soc.* **2001**, *123*, 4029. (b) A. D. D. Tulloch, A. A. Danopoulos, S. Kleinhenz, M. E. Light, M. B. Hursthouse, G. Eastham, *Organometallics* **2001**, *20*, 2027. (c) X. L. Hu, I. Castro-Rodriguez, K. Olsen, K. Meyer, *Organometallics* **2004**, *23*, 755. (d) D. Nemcsok, K. Wichmann, G. Frenking *Organometallics* **2004**, *23*, 3640. (e) L. Gagliardi, C. J. Cramer, *Inorg. Chem.* **2006**, *45*, 9442. (f) S. Saravankumar, A. I. Oprea, M. K. Kindermann, P. G. Jones, J. Heinicke, *Chem. Eur. J.* **2006**, *12*, 3143. (g) W. A. Herrmann, J. Schütz, G. D. Frey, E. Herdtweck, *Organometallics* **2006**, *25*, 2437. (h) L. Mercs, G. Labat, A. Neels, A. Ehlers, M. Albrecht, *Organometallics* **2006**, *25*, 5648. (i) D. M. Khramov, V. M. Lynch, C. W. Bielawski, *Organometallics* **2007**, *26*, 6042. (j) E. F. Penka, C. W. Schläpfer, M. Atanasov, M. Albrecht, C. Daul, *J. Organomet. Chem.* **2007**, *692*, 5709. (k) U. Radius, F. M. Bickelhaupt, *Organometallics* **2008**, *27*, 3410. (l) Khramov, D. M. Rosen, E. L. Er, J. A. V. Vu, P. D. Lynch, V. M. Bielawski, C. W. *Tetrahedron* **2008**, *64*, 6853–6862. (m) H. Jacobsen, A. Correa, A. Poater, C. Costabile, L. Cavallo, *Coord. Chem. Rev.* **2009**, *253*, 687.

[15] (a) O. Guerret, S. Solé, H. Gornitzka, M. Teichert, G. Trinquier, G. Bertrand, *J. Am. Chem. Soc.* **1997**, *119*, 6668–6669. (b) D. M. Khramov, A. J. Boydston, C. W. Bielawski, *Angew. Chem. Int. Ed.* **2006**, *45*, 6186–6189. (c) A. J. Boydston, C. W. Bielawski, *Dalton Trans.* **2006**, 4073–4077. (d) A. Zanardi, R. Corberan, J. A. Mata, E. Peris, *Organometallics* **2008**, *27*, 3570–3576. (e) L. Mercs, A. Neels, H. Stoeckli-Evans, M. Albrecht, *Dalton Trans.* **2009**, 7168–7178. (f) A Zanardi, J. A. Mata, E. Peris, *J. Am. Chem. Soc.* **2009**, *131*, 14531–14537. (g) K. A. Williams, C. W. Bielawski, *Chem. Commun.* **2010**, *46*, 5166. (h) L. Mercs, A. Neels, H. Stoeckli-Evans, M. Albrecht, *Inorg. Chem.* **2011**, *50*, 8188–8196. (i) A. Prades, M. Poyatos, J. A. Mata, E. Peris, *Angew. Chem. Int. Ed.* **2011**, *50*, 7666–7669. (j) M. Schmidtendorf, T. Pape, F. E. Hahn, *Angew. Chem. Int. Ed.* **2012**, *51*, 2195–2198. (k) A. Prades, E. Peris, M. Alcarazo, *Organometallics* **2012**, *31*, 4623–4626. (l) M. T. Zamora, M. J. Ferguson, R. McDonald, M. Cowie, *Organometallics* **2012**, *31*, 5463–5477. (m) S. Sabater, J. A. Mata, E. Peris, *Organometallics* **2012**, *31*, 6450–6456. (n) R. Maity, H. Koppetz, A. Hepp, F. E. Hahn, *J. Am. Chem. Soc.* **2013**, *135*, 4966–4969. (o) R. Maity, A. Rit, C. Schulte to

Brinke, C. G. Daniliuc, F. E. Hahn, *Chem. Commun*. **2013**, *49*, 1011–1013. (p) S. Gonell, M. Poyatos, J. A. Mata, E. Peris, *Angew. Chem. Int. Ed.* **2013**, *52*, 7009–7013.

[16] D. G. Gusev, E. Peris, *Dalton Trans.* **2013**, *42*, 7359–7364.

[17] A. G. Tennyson, E. L. Rosen, M. S. Collins, V. M. Lynch, C. W. Bielawski, *Inorg. Chem.* **2009**, *48*, 6924–6933.

[18] L. Mercs, A. Neels, M. Albrecht, *Dalton Trans.* **2008**, 5570–5576.

[19] O. Schuster, L. Mercs, M. Albrecht, *Chimia* **2010**, *64*, 184–187.

[20] (a) A. Juris, V. Balzani, F. Barigelletti, S. Campagna, P. Belser, A. von Zelewsky, *Coord. Chem. Rev.* **1988**, *84*, 85. (b) C. Kaes, A. Katz, M. W. Hosseini, *Chem. Rev.* **2000**, *100*, 3553–3590 (c) Constable, E. C. *Chem. Soc. Rev.* **2007**, *36*, 246. (d) M. D. Ward, *Chem. Commun.* **2009**, 4487.

[21] A. J. Boydston, P. D. Vu, O. L. Dykhno, V. Chang, A. R. Wyatt, A. S. Stockett, E. T. Ritschdorff, J. B. Shear, C. W. Bielawski, *J. Am. Chem. Soc.* **2008**, *130*, 3143–3156.

[22] (a) A. Prades, M. Viciano, M. Sanau, E. Peris, *Organometallics* **2008**, *27,* 4254–4259. (b) C. Gandolfi, M. Heckenroth, A. Neels, G. Laurenczy, M. Albrecht, *Organometallics.* **2009**, *28*, 5112–5121. (c) L. Bernet, R. Lalrempuia, W. Ghattas, H. Mueller-Bunz, L. Viagara, A. Llobet, M. Albrecht, *Chem. Commun.,* **2011**, 47, 8058–8060.

[23] (a) H. M. J. Wang, I. J. B. Lin, *Organometallics* **1998**, *17*, 972–975. (b) I. J. B. Lin, C. S. Vasam, *Comments Inorg. Chem.* **2004**, *25*, 75–129. (c) J. C. Garrison, W. J. Youngs, *Chem. Rev.* **2005**, *105*, 3978–4008.

[24] (a) J. A. Mata, A. R. Chianese, J. R. Miecznikowski, M. Poyatos, E. Peris, J. W. Faller, R. H. Crabtree, *Organometallics* **2004**, *23*, 1253–1263. (b) T. Zamora, M. J. Ferguson, M. Cowie, *Organometallics* **2012**, *31*, 5384–5395.

[25] (a) R. Le Lagadec, L. Rubio, L. Alexandrova, R. A. Toscano, E. V. Ivanova, R. Meskys, V. Laurinavicius, M. Pfeffer, A. D. Ryabov, *J. Organomet. Chem.* **2004**, *689,* 4820–4832. (b) D. Kuang, S. Ito, B. Wenger, C. Klein, J.-E. Moser, R. Humphry-Baker, S. M. Zakeeruddin, M. Grätzel, *J. Am. Chem. Soc.* **2006**, *128,* 4146–4154. (c) W. Ghattas, H. Mueller-Bunz, M. Albrecht, *Organometallics,* **2010**, *29*, 6782–6789. (d) H.-S. Chen, W.-C. Chang, C. Su, T.-Y. Li, N.-M. Hsu, Y. S. Tingare, C.-Y. Li, J.-H. Shie, W.-R. Li, *Dalton Trans.* **2011**, *40*, 6765–6770. (e) V. Leigh, W. Ghattas, R. Lalrempuia, H. Mueller-Bunz, M. T. Pryce, M. Albrecht, *Inorg. Chem.,* **2013**, *52*, 5395–5402.

[26] (a) A. A. D. Tulloch, A. A. Danopoulos, G. J. Tizzard, S. J. Coles, M. B. Hursthouse, R. S. Hay-Motherwell, W. B. Motherwell, *Chem. Commun.* **2001**, 1270–1271. (b) J. A. Loch, M. Albrecht, E. Peris, J. Mata, J. W. Faller, R. H. Crabtree, *Organometallics* **2002**, *21*, 700–706. (c) V. Khlebnikov, A. Meduri, H. Mueller-Bunz, T. Montini, P. Fornasiero, E. Zangrando, B. Milani, M. Albrecht, *Organometallics* **2012**, *31*, 976–986.

[27] For example, the torsion angle between the vectors of the MeCN ligands *trans* to the carbene, defined by the two least-square planes containing Ru1, N23, N43, N53, and containing Ru1a, N23a, N43a, and N53a, respectively, is 38.84° and thus deviates substantially from an ideally linear geometry (with torsion angle 0°).

[28] (a) T. W. Smith, J. E. Kuder, D. Wychick, *J. Polym. Sci. Polym. Chem. Ed.* **1976**, *14*, 2433–2448. (b) J. B. Flanagan, S. Margel, A. J. Bard, F. C. Anson, *J. Am. Chem. Soc.* **1978**, *100*, 4248–4253.

[29] M. B. Robin, P. Day, *Adv. Inorg. Radiochem.* **1968**, *10*, 247–422.

[30] M. Krejcik, M. Danek, F. Hartl, *J. Electroanal. Chem* **1991**, *317*, 179–187.

[31] D. M. D'Alessandro, F. R. Keene, *Dalton Trans.* **2004**, 3950.

[32] For related borderline class II/III examples, see: (a) K. D. Demadis, C. M. Hartshorn, T. J. Meyer, *Chem. Rev.* **2001**, *101*, 2655. (b) B. J. Lear, S. D. Glover, J. C. Salsman, C. H. Londergan, C. P. Kubiak, *J. Am. Chem. Soc.* **2007**, *129*, 12772. (c) M. Koley, B. Sarkar, S. Ghumaan, E. Bulak, J. Fiedler, W. Kaim, G. K. Lahiri, *Inorg. Chem.* **2007**, *46*, 3736–3742. (d) T. Kurahashi, H. Fujii, *J. Am. Chem. Soc.* **2011**, *133*, 8307. (e) S. D. Glover, C. P. Kubiak, *J. Am. Chem. Soc.* **2011**, *133*, 8721. (f) W.-W. Yang, J. Yao, Y.-W. Zhong, *Organometallics* **2012**, *31*, 1035–1041.

[33] A. B. P. Lever, *Inorg. Chem.* **1990**, *29*, 1271–1285.

[34] W. Kaim, J. Fiedler, *Chem. Soc. Rev.* **2009**, *38*, 3373.

[35] W. R. Browne, R. Hage, J. G. Vos, *Coord. Chem. Rev.* **2006**, *250*, 1653−1668.

[36] R. A. Marcus, *Annu. Rev. Phys. Chem.* **1964**, *15*, 155–196.

[37] S. Barlow, C. Risko, S.-J. Chung, N. M. Tucker, V. Coropceanu, S. C. Jones, Z. Levi, J.-L. Brédas, S. R. Marder, *J. Am. Chem. Soc.* **2005**, *127*, 16900–16911.

[38] N. G. Connelly, W. E. Geiger, *Chem. Rev.* **1996**, *96*, 877–910.

[39] G. M. Sheldrick, *Acta Cryst. A* **2007**, *64*, 112–122.

[40] A. L. Spek, *Acta Cryst. D* **2009**, *65*, 148–155.

Supporting Information

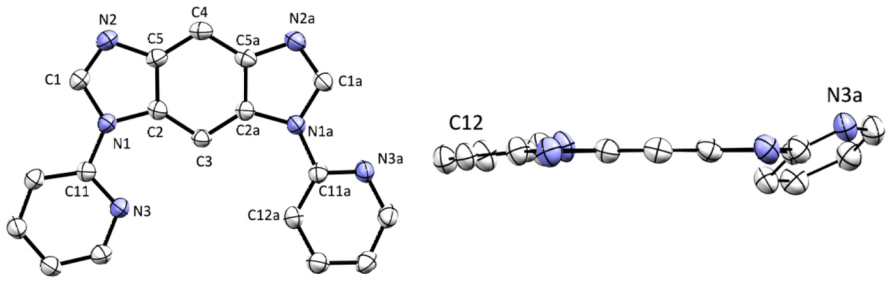

Figure S1a. ORTEP View of **2** (ellipsoids at the 50% probability level). Hydrogen atoms have been omitted for clarity.

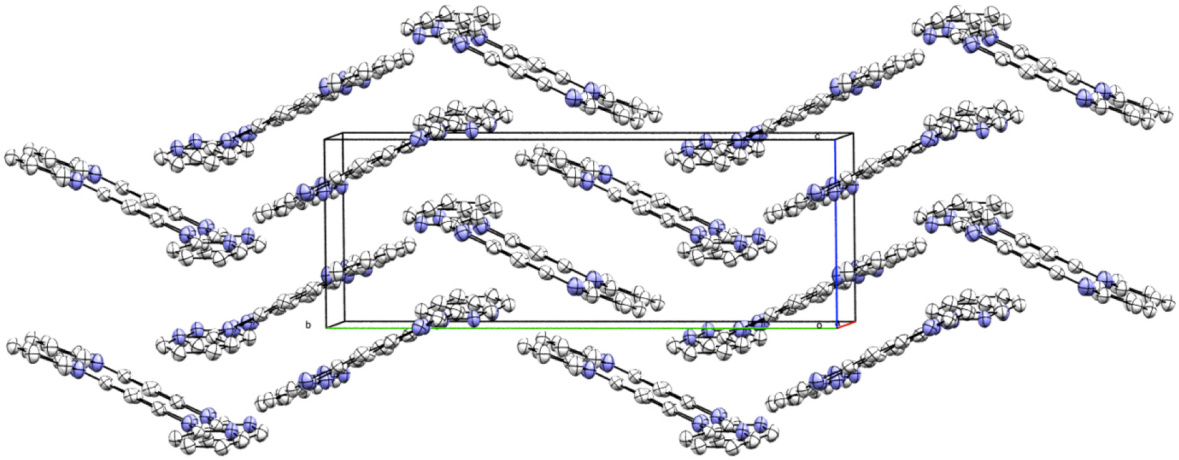

Figure S1b. Packing diagram of compound **2** seen along the a-axis (ellipsoids at the 50% probability level). Hydrogen atoms have been omitted for clarity.

Table S1. Selected interatomic distances (Å) and angles (°) for compound **2**.

C1–N1	1.3808(17)	C5–C4	1.388(2)
C1a–N1a	1.3787(17)	C5a–C4	1.386(2)
C1–N2	1.2968(19)	N1–C11	1.4150(17)
C1a–N2a	1.2983(19)	N1a–C11a	1.4172(17)
N1–C2	1.3976(17)		
N1a–C2a	1.4000(17)	N1–C1–N2	114.4(1)
N2–C5	1.3965(18)	N1a–C1a–N2a	114.7(1)
N2a–C5a	1.4107(19)	C1–N1–C11	124.3(1)
C2–C3	1.3879(18)	C1a–N1a–C11a	125.9(1)
C2a–C3	1.3852(19)		
C2–C5	1.4136(18)	C1…C1a	6.449(2)
C2a–C5a	1.4107(19)		

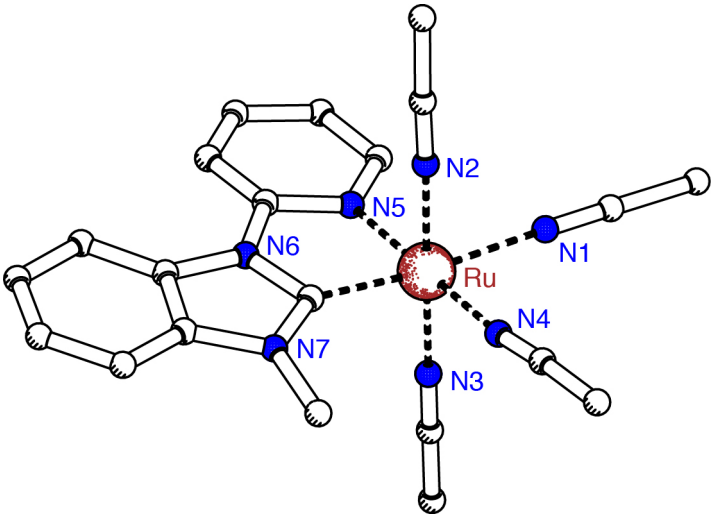

Figure S2. Pluton drawing of one of the four crystallographically independent complex cations of **9**. Severe disorder in the anions could not be refined to acceptable levels, which prevents a full discussion of data. The bite angle of **9** is in the expected range (78.5° in average over the four independent residues, cf Table 2). The bonds between the ruthenium center and the solvent ligands also follow the same trend as observed in **6**, with the MeCN trans to the carbene markedly more distant from the Ru center than the other three MeCN ligands: Ru–C1 1.97; Ru–N1 2.12; Ru–N2 2.04; Ru–N3 2.03; Ru–N4 2.01; Ru–N5 2.06;

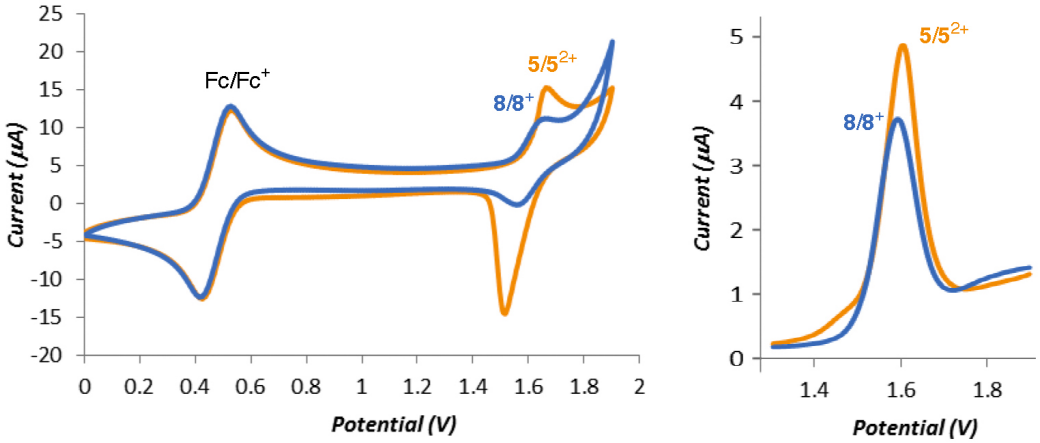

Figure S3.CV diagram (left) and DPV measurement (right) of complexes **5** and **8** (ca. 1 mM) in dry CH_2Cl_2 with 0.1 M $[NBu_4][PF_6]$ as supporting electrolyte at 100 mV s^{-1} scan rate; Fc^+/Fc used as internal reference.

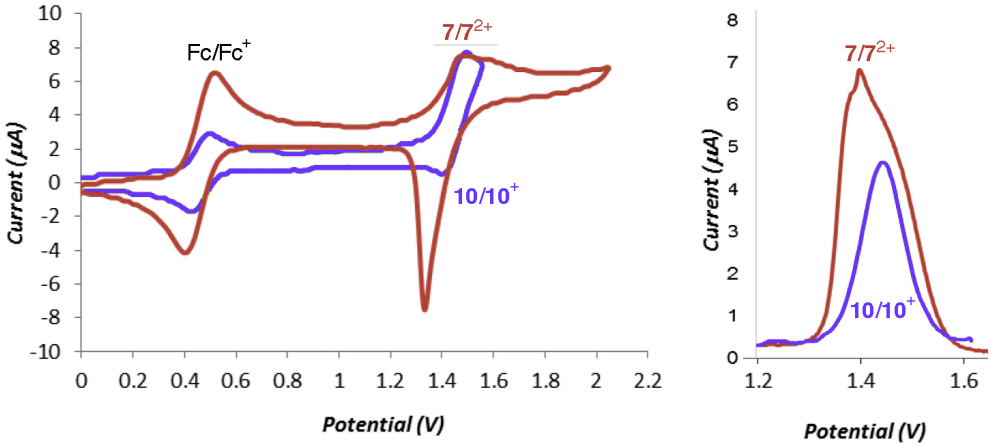

Figure S4. CV (left) and DPV (right) plot of complexes **7** and **10** (ca. 1 mM) in dry CH_2Cl_2 with 0.1 M $[NBu_4][PF_6]$ as supporting analyte, 50 mV s^{-1} scan rate (Fc^+/Fc used as internal standard, $E_{1/2}$ (Fc/Fc^+) = 0.41 V vs. SCE).

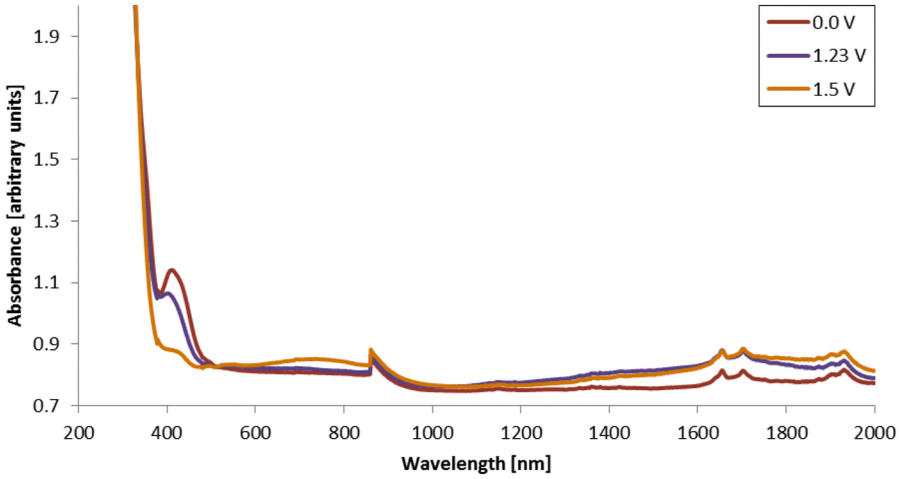

Figure S5. Absorption spectra of complexes **7** at 0.0 V, 7^+ at +1.23 V and $\mathbf{7}^{2+}$ at +1.5 V ($MeNO_2$ solution).

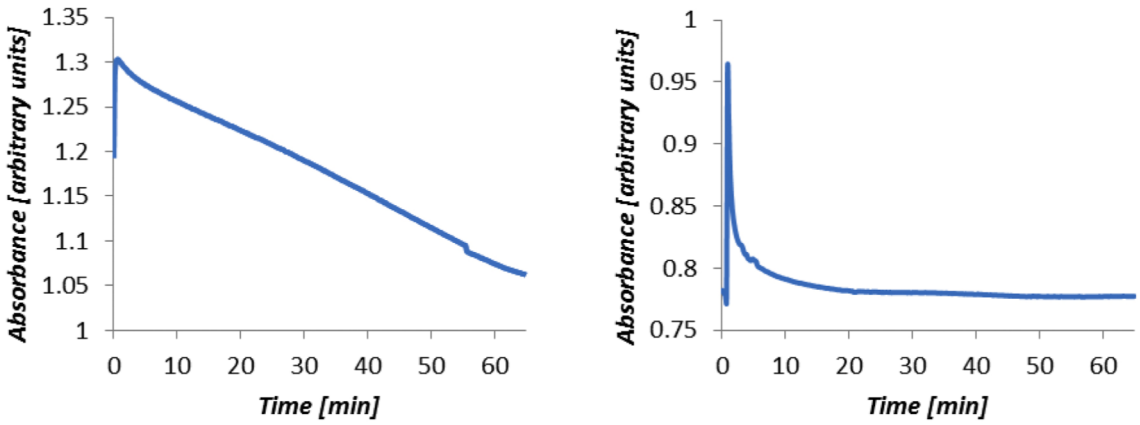

Figure S6. Stability tests: MV species $\mathbf{6}^{+}$ at 1.46 V observed at 1590 nm (left). Fully oxidized $\mathbf{6}^{2+}$ species at 1.6 V observed at 820 nm (right).

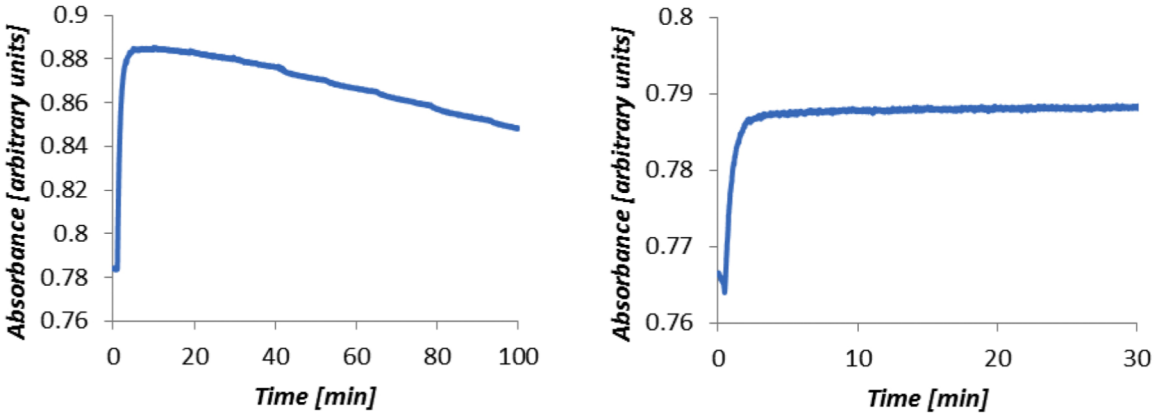

Figure S7. Stability tests: MV species $\mathbf{7}^{+}$ at 1.23 V observed at 1730 nm (left).Dication $\mathbf{7}^{2+}$ at 1.5 V observed at 740 nm (right).

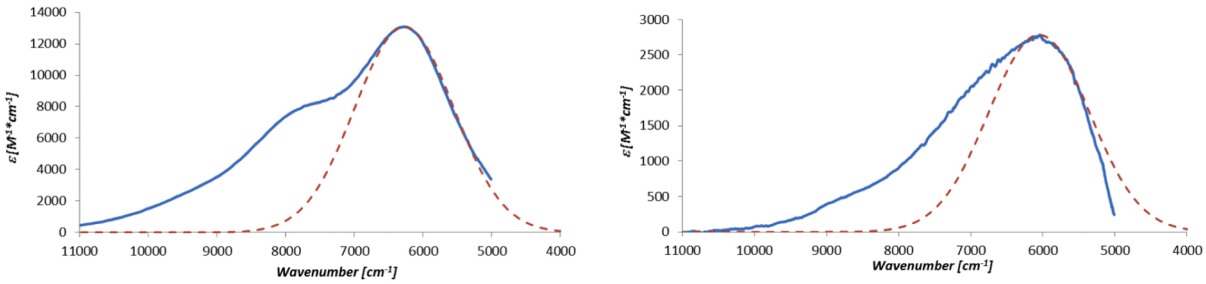

Figure S8. IVCT band of the mixed-valent species $\mathbf{6}^{+}$ (left) $\mathbf{7}^{+}$ (right; blue solid lines) and corresponding (symmetric) Gaussian fitting curves (red dashed lines). The poor fit demonstrates the asymmetric shape of the IVCT band.

Table S2. Crystallographic data for compounds **2**, **6**, and **10**.

	2	**6**	**10**
CCDC No.			
mol formula	$C_{18}H_{12}N_6$	$C_{52}H_{64}F_{24}N_{22}P_4Ru_2$	$C_{33}H_{27}F_{12}N_7P_2Ru$
Crystal system	Monoclinic	Monoclinic	Triclinic
Space group	$P2_1/c$	$P2_1/c$	P_{-1}
Unit cell			
a /Å	9.2616(4)	12.154(2)	10.4632(9)
b /Å	20.3317(6)	28.597(6)	12.4848(13)
c /Å	7.5352(3)	21.640(4)	18.8260(15)
α /°	90	90	97.959(8)
β /°	96.336(3)	90.03(3)	103.187(6)
γ /°	90	90	114.396(6)
Volume /Å^3	1410.24(9)	7521(3)	2104.2(3)
Z	4	4	2
T /K	200	100	150
μ /mm^{-1}	0.09	0.60	0.79
Abs. corr.	none	numerical	Numerical
Total reflecns	19196	13538	15954
Unique reflecns	2652	13538	7309
parameters	217	956	551
R_1[a)] [I>2σ(I)]	0.0388,	0.0657	0.0585
wR_2[b)] [I>2σ(I)]	0.1024	0.1556	0.1401
GOOF	1.048	0.979	1.049
ρ_{fin} (max, min) /e Å^{-3}	0.18, –0.20	0.77, –0.87	0.81, –0.69

[a)] $R_1 = \Sigma||F_O|-|F_C||/\Sigma|F_O|$.

[b)] $wR_2 = [\Sigma w(F_O^2-F_C^2)^2/\Sigma(w(F_O^2)^2)]^{1/2}$; $w = 1/[\sigma^2(F_O^2) + (ap)^2 + bp]$; $p = (F_O^2 + 2F_C^2)/3$.